Eindhoven University of Technology

MASTER

Design and experimental results of synchronizing metronomes, inspired by Christiaan Huygens

Oud, W.T.

Award date:
2006

Link to publication

Design and experimental results of synchronizing metronomes, inspired by Christiaan Huygens

Ward T. Oud

DCT 2006.20

Master's thesis

Coaches: Prof.dr. H. Nijmeijer
                dr. A.Y. Pogromsky

Supervisor: Prof.dr. H. Nijmeijer

Committee: Prof.dr. H. Nijmeijer
                dr. A.Y. Pogromsky
                dr.ir. N. Rosielle
                dr.ir. P.D. Anderson

Eindhoven University of Technology
Department of Mechanical Engineering
Dynamics and Control group

Eindhoven, February, 2006

Errata

- In the figures 5.4, 5.5, 5.6, 6.1b, 6.3, 6.4, 6.6b, 6.7, 6.8, 6.10 and 6.11 the unit of the phase difference plot on the vertical axis should not read "[rad]", but "[π rad]".

- In the figures 6.2 and 6.9 the unit of the angle θ is missing, the complete label should be "θ [rad]".

Abstract

Inspired by the observation of synchronization of two pendulum clocks by Christiaan Huygens, a comparable experimental setup is designed and analyzed in this report. Instead of using pendulum clocks, metronomes have been used as oscillators in the setup. Coupling between the metronomes is introduced in the system by horizontal translation of the connecting platform.

After description of the design of the experimental setup and the measurement methods, a model is proposed which is used to analyze the system. The model consists of two driven pendula attached to a mass which is connected to the outside world by a linear spring and damper. The escapement, which provides energy input to the metronomes, is modeled as a sinusoidal shaped torque between fixed angles. Given the dynamical model, the parameters of the system are estimated from experiments using a nonlinear Kalman filter and the results are validated.

Synchronization experiments have been performed for two distinct configurations of the system. First synchronization of the metronomes has been investigated for a relative eigenfrequency of the platform approximately twice as large as the frequency of the metronomes. In this configuration only anti-phase synchronization is observed. When the relative eigenfrequency of the platform is almost equal to the metronomes' frequency, both in- and anti-phase synchronization is possible, depending on the parameters of the system. Finally the results obtained in the experiments are reproduced qualitatively in simulations with the dynamical model.

Contents

**Design and experimental results
of synchronizing metronomes,
inspired by Christiaan Huygens**

Chapter 1

Introduction

1.1 Synchronization in history

One of the first documented observations of synchronization is by the Dutch scientist Christiaan Huygens. In the 17th century maritime navigation called for more accurate clocks in order to determine the position of a ship on sea. Christiaan Huygens' solution for precise timekeeping was the invention of the pendulum clock (Yoder 1988). During some time Huygens was bound to his home due to illness, he observed that two pendulum clocks, attached to the same beam supported by chairs, would swing in exact opposite direction after some time (Huygens 1893, 1932, 1986). A drawing made by Christiaan Huygens is given in figure 1.1. Disturbances or different initial positions did not affect the synchronous motion which resulted after about half an hour. This effect which Huygens called *"sympathie des horloges"* is nowadays know as synchronization and is characterized by Pikovsky et al. (2001) as *"an adjustment of rhythms of oscillating objects due to their weak interaction"*. The oscillating objects in Huygens' case are two pendulum clocks and are weakly coupled through translation of the beam.

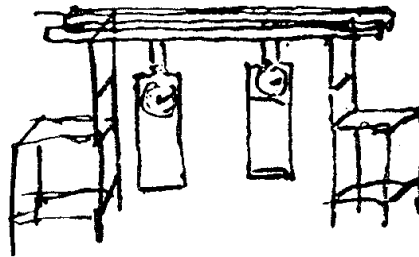Many more cases of synchronization have been identified in nature and tech-

Figure 1.1: Drawing by Christiaan Huygens of two pendulum clocks attached to a beam which is supported by chairs. Synchronization of the pendula was observed by Huygens in this setup. From (Huygens 1932).

nology around us. A striking example in biology is the synchronized flashing of fireflies Buck (1988). A better understanding of synchronization might also help gaining insight into the working of the human brain. The occurrence of synchronization in relation to the retrieval of stored patterns in the brain is hypothesized by Von Der Malsburg (1999). Experimentally, synchronization has been shown in EEG studies of cat brains by Gray et al. (1989).

Synchronization is also found in technology, for example the frequency synchronization of triode generators. These generators were the basic elements of early radio communication systems Appleton (1922). Using synchronization it is possible to stabilize the frequency of a high power generator with a precise, low power one.

1.2 Problem definition

Three centuries later the phenomenon of synchronizing driven pendula is, to our best knowledge, repeated twice experimentally. In the first research by Bennett et al. (2002), one has tried to accurately reproduce the findings of Huygens in an experimental setup consisting of two pendulum clocks attached to a freely moving cart. The results of this experiment confirm the documented observations of Christiaan Huygens. A rather simple but interesting experiment is described by Pantaleone (2002), where synchronization of two metronomes is discussed, which are coupled by a wooden board rolling on soda cans. The metronomes in this setup would synchronize most of the time with in-phase oscillations. However when extra damping was added to the base, also anti-phase synchronization was observed. A photo of the setup is given in figure 1.2.
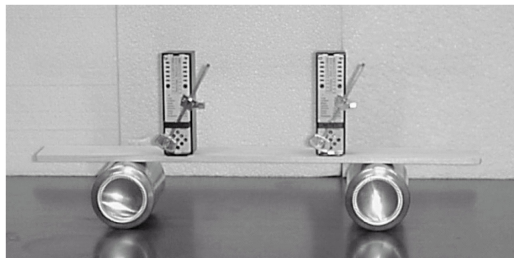
Figure 1.2: Setup with two metronomes coupled by a wooden board rolling on soda cans. In contrast to the findings of Christiaan Huygens mostly in-phase synchronization was observed. From (Pantaleone 2002). .

The research presented in this report is inspired by the observations of Christiaan Huygens, the work of Bennett et al. (2002) and Pantaleone (2002). The main objective will be to perform and analyze synchronization experiments with a setup consisting of driven pendula. This problem will be subdivided in the following steps:

- Design a mechanical setup with two metronomes and a coupling medium.

- Choose a measurement system for the oscillation of the metronomes and movement of the coupling medium.

- Derive, identify and verify a model for the experimental setup.

- Perform synchronization experiments with the setup.

- Evaluate and compare the synchronization experiments with simulations.

1.3 Report outline

The report will be organized in the following order, first in chapter 2 the experimental setup is described. In this chapter the design of the setup and the measurement methods are discussed. When this is treated, a mathematical model describing the setup is introduced. Especially the modeling of the metronomes used in the experiments is given attention. Identification of the setup with the derived model is discussed in chapter 4. In the next chapter the synchronization experiments are treated. Combining the results of the identification and the experiments, synchronization simulations are discussed in chapter 6. Finally the conclusions from the project are drawn and recommendations for further research are given.

Chapter 2

Experimental setup

The design of the experimental setup is described in this chapter. First the concept and the individual parts of the setup are discussed, finally the measurement methods are given attention. The basic idea of the setup is to be able to perform synchronization experiments with two oscillators which are coupled mechanically. Due to the coupling the oscillators influence each other and can synchronize.

In order to keep the setup simple and cheap, two off the shelf metronomes, which are normally used for indicating a rhythm for musicians, are chosen as oscillators. Coupling between the metronomes is obtained by mounting them on a platform which can translate in horizontal direction. A photograph of the experimental setup is given in figure 2.1.
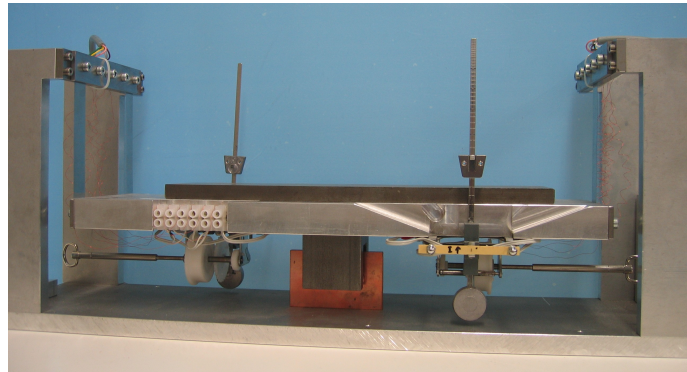

Figure 2.1: Photograph of the experimental setup.

2.1   Metronomes

The metronomes are made by Wittner, type Maelzel (series 845) and consist of a pendulum and a driving mechanism, called the escapement. The energy lost due

to friction is compensated by this escapement. A photograph of a metronome is given in figure 2.2 indicating the various parts. The escapement consists of a spring which loads a toothed wheel. These teeth have a V-shape and alternately push away one of the two cams fixed to the axis of the pendulum. The typical "tick-tack" sound of mechanical metronomes is produced each time the next teeth hits a cam.

The frequency of the metronomes can be adjusted with a counterweight attached to the upper part of the pendulum. Variation of the frequency between 2.4 rad/s and 10.8 rad/s is possible with the weight attached, without it the frequency of the metronomes increases to 12.3 rad/s. The amplitude of the metronomes' oscillations cannot be influenced, however at increasing frequencies the amplitude decreases.
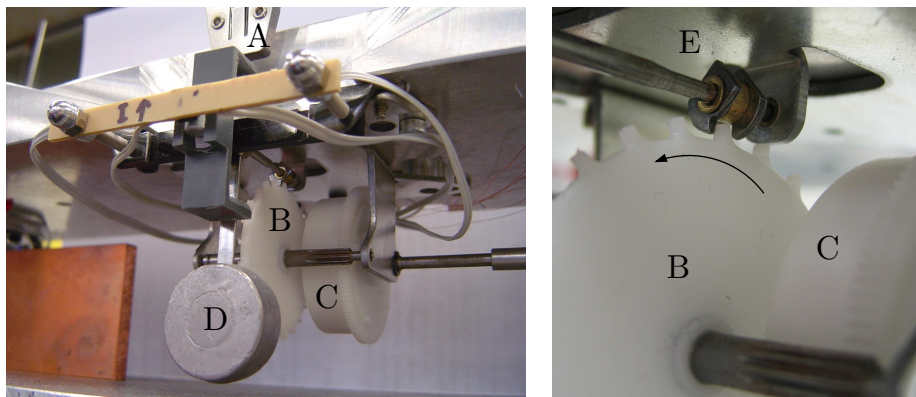

Figure 2.2: Photograph of one of the metronomes on the left and a close up of the axis of the pendulum on the right. The main parts of the metronome are the counterweight of the pendulum (A), toothed wheel with cams above it (B), torsional spring (C) and the pendulum with a weight on its end (D). On the right the cams which are fitted to the axis of the pendulum (E) are visible. The toothed wheel (B) loads the cams in the indicated direction by the torsional spring (C).

2.2   Platform

The platform does not only act as a support for the metronomes but because of its possible horizontal translation it couples the dynamics of both metronomes as well. In order to keep the equations of motion of the total system simple a suspension with linear stiffness and damping is desired. Regarding the dimensions of the platform, only the resulting weight is important, as this parameter influences the coupling strength between the metronomes. Based on the results in Bennett et al. (2002), Pantaleone (2002), a weight of approximately 2 kg is chosen for the platform. With additional iron bars the mass of the platform can be increased easily afterwards. Considering the desired mass and enough place to install the metronomes, the length, width and thickness of the platform are respectively 345, 95 and 20 mm.

As long as the translation of the platform is not too large (mm range) the use of leaf springs makes a frictionless translation possible with linear stiffness and
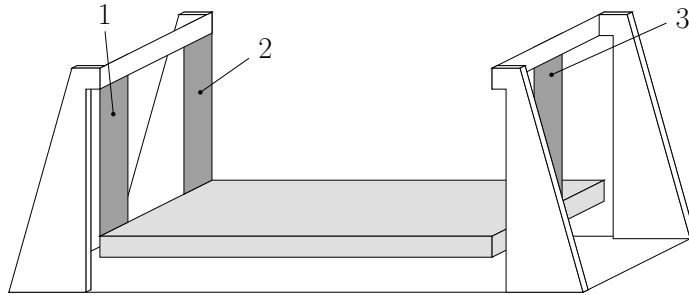
Figure 2.3: Placement of the three leaf springs between the platform and the supporting frame.

damping properties (Rosielle & Reker 2000). In the initial design the leaf springs had a width equal to that of the platform. Installing these leaf springs turned out to be impossible without buckling them due to small errors in alignment of the platform with the frame. To solve this problem, the broad leaf springs are replaced by three smaller leaf springs in the configuration depicted as 1,2,3 in figure 2.3. When the platform is installed carefully, so that the leaf springs do not buckle and the platform is horizontal, the stiffness and damping of the leaf springs show a linear behavior.

In order to calculate the necessary dimensions for leaf springs the following estimates have been used. The stiffness of a leaf spring can be estimated by assuming it behaves as two bars clamped at one side. For small deflections the stiffness of a bar clamped at one side is given by Fenner (1989)

$$k = \frac{Ehb^3}{4L^3}, \tag{2.1}$$

where E is the elastic modulus, h the width, b the thickness and L the length of the bar. The leaf spring has a stiffness equal to (2.1) since both halves of the leaf spring take half the deflection and half the force. The eigenfrequency of the platform in rad/s is estimated by

$$\Omega = \sqrt{\frac{Ehb^3}{4(l/2)^3 M} + \frac{g}{l}} \tag{2.2}$$

where l is the length of the leaf spring, M the mass of the platform and g the constant of gravity. For the setup the following dimensions for the leaf springs are chosen: l=80 mm, b=0.4 mm and h=15+15+10 mm (three leaf springs). The constants are $E = 200 \cdot 10^9$ kg/m/s^2 and g=9.81 m/s^2. The platform has a mass of 2.35 kg which results in an eigenfrequency of approximately 31 rad/s.

2.3   Measurements

In the setup the angle of the metronomes and the translation of the platform are of interest. Since alteration of the dynamics of both the metronomes and the platform should be avoided, contactless measurement methods have

been chosen. All signals are recorded using a Siglab data acquisition system, model 20-42. First the measurement of the metronomes is discussed, secondly that of the translation of the platform.

The angle of the metronomes is measured using a sensor based on the anisotropic magnetoresistance (AMR) principle, described eg. in *Applications of magnetic position sensors* (2002), *Linear/angular/rotary displacement sensors* (2003). The resistance of AMR materials changes when a magnetic field is applied. Above a minimal field strength the magnetization of the material saturates and aligns with the external field and the following relation holds for the resistance R

$$R \sim \cos^2 \theta \tag{2.3}$$

where θ is the angle between the magnetic field and the current through the resistor. By combining four AMR resistors in a bridge of Wheatstone a change in resistance is converted to a voltage difference. Two of these bridges of Wheatstone are located in the sensor, but are rotated 45° degrees with respect to each other. As a result the voltage difference of bridges A and B can be written as

$$\Delta V_A = V_s S \sin 2\theta \,, \quad \Delta V_B = V_s S \cos 2\theta \tag{2.4}$$

where V_s is the voltage supplied to the bridges and S is the AMR material constant. The angle θ can be calculated from these signals by

$$\theta = \tfrac{1}{2} \arctan(\Delta V_A / \Delta V_B) \tag{2.5}$$

regardless of the value of voltage V_s and constant S. Due to manufacturing tolerances the bridges will show an offset when no magnetic field is applied. This offset can be corrected in software when both signals are recorded.

In the experimental setup the AMR sensor is mounted on the platform and a small permanent magnet is attached to the pendulum. In order to obtain a strong magnetic field a Neodymium magnet is used. From both sensors electrical wires have to be guided from the platform to the outside world. In an early setup these wires were relatively thick and introduced considerable nonlinear damping to the platform. In order to solve this problem, thinner wires and a routing along the leaf springs was chosen. This approach solved the problem of nonlinear damping.

The position and velocity of the platform is measured using a Polytec Vibrometer, type OFV 3000 with a OFV 302 sensorhead. The position measurement is based on interferometry, the velocity measurement on the Doppler shift of a laser beam reflected on the platform.

Chapter 3

Model

The model used for identification and analysis of the system will be discussed in this chapter. The setup will be modeled as two non-identical driven pendula attached to a mass which is connected to the outside world by a spring and damper. A schematic drawing of the setup is given in figure 3.1. First, using Lagrange's formalism, the equations of motion will be derived and secondly a model for the escapement of the metronomes will be proposed.
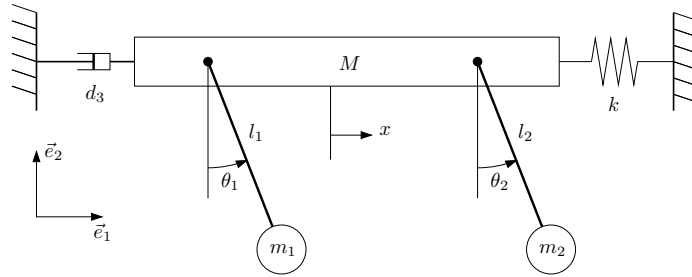
Figure 3.1: Schematic drawing of the setup, which consists of two pendula with mass m_i and length l_i attached to the platform with mass M. The platform is suspended by a spring and damper. The degrees of freedom of the system are the angle θ_i and the translation x in horizontal direction.

3.1 Equations of motion

Assuming the setup consists of rigid bodies the equations of motion can be derived using Lagrangian mechanics, see eg. De Kraker & Van Campen (2001). The generalized coordinates are chosen as

$$\underline{q}^T = [\theta_1, \theta_2, x] \tag{3.1}$$

which are the angles of the pendula and the translation of the platform. The kinetic energy $T(\underline{q}, \underline{\dot{q}})$ of the system can be expressed as

$$T(\underline{q}, \underline{\dot{q}}) = \tfrac{1}{2} m_1 \dot{\vec{r}}_1 \cdot \dot{\vec{r}}_1 + \tfrac{1}{2} m_2 \dot{\vec{r}}_2 \cdot \dot{\vec{r}}_2 + \frac{1}{2} M \dot{\vec{r}}_3 \cdot \dot{\vec{r}}_3 \tag{3.2}$$

where r_1, r_2 and r_3 are respectively the translation of the center of mass of pendulum I, II and the platform, m_1 and m_2 are the mass of pendulum I and II, l_1 and l_2 the lengths of the center of mass to the pivot point of pendulum I and II, M is the mass of the platform and

$$\vec{r}_1 = (x + l_1 \sin\theta_1) \cdot \vec{e}_1 - l_1 \cos\theta_1 \cdot \vec{e}_2 \tag{3.3a}$$

$$\vec{r}_2 = (x + l_2 \sin\theta_2) \cdot \vec{e}_1 - l_2 \cos\theta_2 \cdot \vec{e}_2 \tag{3.3b}$$

$$\vec{r}_3 = x \cdot \vec{e}_1 \tag{3.3c}$$

The potential energy $V(\underline{q})$ of the system consists of gravity acting on the pendula and the energy stored in the spring,

$$V(\underline{q}) = m_1 g l_1 (1 - \cos\theta_1) + m_2 g l_2 (1 - \cos\theta_2) + \tfrac{1}{2} k x^2 \tag{3.4}$$

where g is the constant of gravity and k is the spring stiffness of the platform. The generalized forces $\underline{Q}^{nc}$ include viscous damping in the hinges of the pendula and the platform and a torque f_i exerted by the escapement on the pendula and can be written as

$$\underline{Q}^{nc} = \begin{bmatrix} f_1 - d_1 \dot{\theta}_1 \\ f_2 - d_2 \dot{\theta}_2 \\ -d_3 \dot{x} \end{bmatrix} \tag{3.5}$$

where d_i are the viscous damping constants of respectively the two pendula and the platform. With Lagrange's equations of motions

$$\frac{d}{dt} \frac{\partial T}{\partial \underline{\dot{q}}} - \frac{\partial T}{\partial \underline{q}} + \frac{\partial V}{\partial \underline{q}} = \left(\underline{Q}^{nc} \right)^T \tag{3.6}$$

the equations of motion for the system become

$$m_1 l_1{}^2 \ddot{\theta}_1 + m_1 l_1 g \sin\theta_1 + m_1 l_1 \cos(\theta_1)\ddot{x} + d_1 \dot{\theta}_1 = f_1 \tag{3.7}$$

$$m_2 l_2{}^2 \ddot{\theta}_2 + m_2 l_2 g \sin\theta_2 + m_2 l_2 \cos(\theta_2)\ddot{x} + d_2 \dot{\theta}_2 = f_2$$

$$M\ddot{x} + d_3 \dot{x} + kx + \sum_{i=1}^{n} m_i l_i \left(\ddot{\theta}_i \cos\theta_i - \dot{\theta}_i^2 \sin\theta_i \right) = 0.$$

These equations for the metronomes can be simplified by dividing all terms by $m_i l_i{}^2$, which give for $i = 1, 2$

$$\ddot{\theta}_i + \omega_i{}^2 \sin\theta_i + \frac{1}{l_i} \cos(\theta_i)\ddot{x} + \frac{d_i}{m_i l_i{}^2} \dot{\theta}_i = \frac{1}{m_i l_i{}^2} f_i \tag{3.8}$$

where $\omega_i = \sqrt{g/l_i}$.

The equations of motion can be written in dimensionless form using the following transformations. The dimensionless time is defined as $\tau = \omega t$ and the position of the platform as $y = x/l = x\omega^2/g$, where $\omega = \frac{1}{2}(\omega_1 + \omega_2)$ is the mean frequency of both pendula. The derivatives of the angles with respect to the dimensionless time are written as θ' and the following relations hold

$$\frac{d\theta}{dt} = \frac{d\theta}{d\tau} \frac{d\tau}{dt} = \omega\theta', \quad \frac{d^2\theta}{dt^2} = \omega^2\theta''.$$

The equations of motion now become

$$\theta_i'' + \gamma_i^2 \cos\theta_i y'' + \gamma_i^2 \sin\theta_i + \delta_i \theta_i' = \epsilon_i \, f_i \qquad (3.9)$$

$$y'' + 2\Omega\xi y' + \Omega^2 y + \sum_{i=1}^{2} \beta_i \gamma_i^{-2} \left(\cos\theta_i \theta_i'' - \sin\theta_i \theta_i'^2 \right) = 0,$$

with coupling parameter $\beta_i = \frac{m_i}{M}$, scaled eigenfrequency of the metronomes $\gamma_i = \omega_i/\omega$, damping factor $\delta_i = \frac{d\omega_i^2}{m_i g}$, forcing parameter of the escapement $\epsilon_i = \frac{\omega_i^4}{m_i g^2}$, eigenfrequency of the platform $\Omega^2 = \frac{k}{M\omega^2}$ and damping ratio of the platform $\xi = \frac{d_3}{2\sqrt{kM}}$.

3.2 Escapement

So far the escapement has been indicated by the unknown function f_i. In order to be able to simulate the response of the setup the following model is proposed. As described in section 2.1 and illustrated in figure 2.2, the escapement of a metronome operates by pushing away cams on the axis of the pendulum.

Without deriving an accurate mechanical model of the escapement it is assumed the escapement operates between two fixed angles and does not depend on the speed of the pendulum. In order to keep the model continuous a sinusoidal function is chosen, which function value and first derivative is zero at its boundaries. The following expression is used for function f

$$f(\theta, \theta') = \begin{cases} 0, & \theta < \phi \vee \theta > \phi + \Delta\phi \\ \frac{1 - \cos(2\pi \frac{\theta - \phi}{\Delta\phi})}{2\Delta\phi}, & \phi \leq \theta \leq \phi + \Delta\phi \wedge \theta' > 0 \end{cases} \qquad (3.10)$$

where ϕ and $\phi + \Delta\phi$ are the angles between which the mechanism works. In figure 3.2 the torque of the escapement is plotted versus time when the pendulum would follow a sinusoidal trajectory.
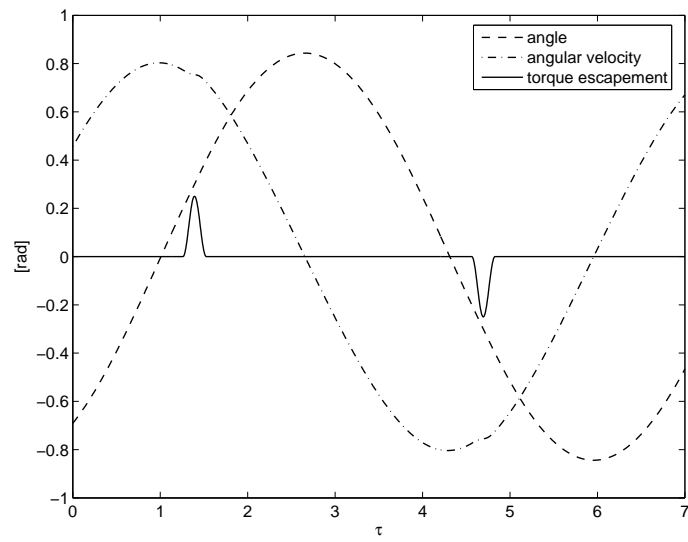
Figure 3.2: The torque exerted by the escapement on the pendulum is plotted versus time together with the angle and velocity of the pendulum. Since the model is dimensionless all signals are in radians.

Chapter 4

Identification

The model derived in the previous chapter will be used to identify the parameters of the experimental setup. This will be done in three parts, first the parameters of the platform will be identified. For this purpose the pendula of the metronomes are held at a fixed angle. Secondly the identification of the metronomes will be discussed. Now the platform is held at rest to avoid influence of the platform and coupling of the metronomes. Finally the coupling between the metronomes and the platform will be estimated. One of the metronomes is fixed and the response of the other oscillating metronome and the platform is measured.

4.1 Platform

When the pendula of the metronomes are fixed to the platform, the setup becomes a single degree of freedom mass-spring-damper system. When the terms relating to the oscillation of the metronomes are removed from (3.7), the equations of motion for the platform become

$$M\ddot{x} + d_3\dot{x} + kx = 0. \tag{4.1}$$

This equation can be written into a form equivalent to (3.9)

$$\ddot{x} + 2\tilde{\Omega}\xi\dot{x} + \tilde{\Omega}^2 x = 0 \tag{4.2}$$

were $\tilde{\Omega} = \omega\Omega$ is the eigenfrequency of the platform in rad/s, whereas the eigenfrequency Ω used in the equations of motion (3.9) is dimensionless.

Since the differential equation (4.2) is linear a solution can be found explicitly

$$x(t) = x(0)e^{-\tilde{\Omega}\xi t}\cos(\tilde{\Omega}\sqrt{1-\xi^2}\,t). \tag{4.3}$$

Using the Hilbert transformation, introduced in appendix C, the amplitude and phase of an oscillating signal can be calculated. From these signals of either the velocity or the position of the platform, the damping and eigenfrequency of the system can be extracted. When plotted on a logarithmic scale the slope, named

Table 4.1: Mass, eigenfrequency and dimensionless damping factor of the platform obtained from the experiments.

M [kg]	$\tilde{\Omega}$ [rad/s]	ξ [‰]
2.35	21.78	0.80
2.35	21.80	0.77
2.35	21.80	0.80
3.16	19.73	0.75
3.96	18.43	0.72
3.96	18.41	0.69
4.36	17.90	0.66
4.77	17.46	0.71
5.16	17.09	0.66
5.76	16.59	0.75
6.17	16.32	0.65
6.56	16.07	0.66
6.98	15.84	0.64
7.37	15.64	0.65
8.18	15.28	0.64

b, of the amplitude versus time is equal to $-\tilde{\Omega}\xi$. The damped eigenfrequency, $\tilde{\Omega}_d = \tilde{\Omega}\sqrt{1 - \xi^2}$ and can be calculated from the slope of the phase versus time.

The dimensionless damping coefficient and the eigenfrequency can be derived from b and $\tilde{\Omega}_d$ by

$$\tilde{\Omega} = \sqrt{b^2 + \tilde{\Omega}_d^2}$$
$$\xi = b/\tilde{\Omega}.$$

(4.4)

The experiments are performed by giving the platform a push by hand and measuring the response. The recorded oscillation after the excitation is the natural response of the platform described by (4.3) and using the Hilbert transform the damping factor and eigenfrequency can be calculated. The decay is the slope of the amplitude on a logarithmic scale versus time, fitted with the least squares method. The eigenfrequency can be obtained from the phase of the Hilbert transform by estimating the slope of the phase in time with a least square fit.

The experiment is performed multiple times with different masses on top of the platform. The results are summarized in table 4.1 and a typical experiment is plotted in figure 4.1, showing the amplitude and phase of the measured velocity of the platform. The mass of the platform is 3.96 kg in this experiment, which results in an eigenfrequency of 18.43 rad/s and a dimensionless damping factor of 0.72 ‰.

The position signal has a higher noise level than the velocity measurement which can be explained by the fact that the position is measured by counting fringes. Especially at low amplitude the discrete steps start to effect the accuracy of the measurement. For this reason the velocity measurements are used for calculating the damping factor and the eigenfrequency.
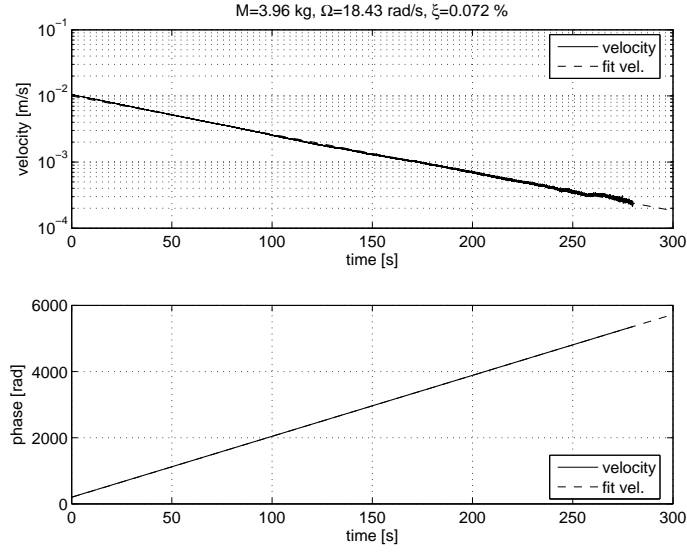
Figure 4.1: Measurement of the velocity of the platform after a displacement of about 0.5 mm. The mass of the platform is 3.96 kg in this experiment. In the upper plot the amplitude of the velocity is plotted on a logarithmic scale versus time. Below is the phase of the velocity signal plotted, used for determining the eigenfrequency of the platform.

Varying the mass of the platform will influence the dynamic properties since the reciprocal mass can be found in both the eigenfrequency and the dimensionless damping factor. If the translational stiffness of the platform is assumed to consist of a spring stiffness and a pendulum effect of the leaf springs, the following relations hold

$$\tilde{\Omega}^2 = k_s \frac{1}{M} + \frac{g}{L}$$
$$\xi\tilde{\Omega} = \frac{d_3}{2} \cdot \frac{1}{M}$$

(4.5)

were k_s is the stiffness, L the length of the leaf springs and g the constant of gravity. When $\tilde{\Omega}^2$ and $\xi\tilde{\Omega}$ are plotted versus $1/M$ in figure 4.2 together with a least-square fit, the linear relationships of (4.5) can be seen. The fit of $\tilde{\Omega}$ however does not go through the origin, indicating the damping is not purely viscous.
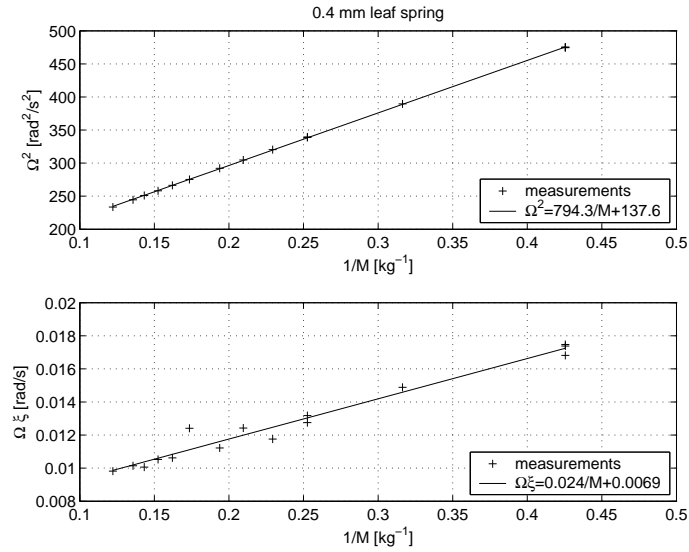
Figure 4.2: Variation of the mass M of the platform influences the eigenfrequency and the product of the dimensionless damping factor and the eigenfrequency. A linear relationship between both $\tilde{\Omega}^2$ and $\xi\tilde{\Omega}$ versus $1/M$ is expected.

4.2 Metronomes

The second part of the experimental setup that has to be identified consists of the metronomes. In chapter 3 the metronomes are modeled as a pendulum with a driving mechanism called the escapement.

Kalman filter

Since the model of the metronomes is nonlinear, a different method has to be used to estimate the parameters of the metronomes. A popular technique is the Kalman filter, see eg. Gelb et al. (2001), which produces optimal, unbiased and consistent estimations of the system states for linear systems. The filter is optimal in the sense that the difference between the actual and estimated state is minimized. However since the system is nonlinear and parameters have to be estimated, a nonlinear extension of the Kalman filter is used. First the basics of the Kalman filter are introduced.

Consider the following nonlinear discrete model which state x_k is to be estimated

$$
\begin{aligned}
x_{k+1} &= f(x_k, u_k, v_k), & v_k &\sim N(0, Q(k)) \\
y_k &= g(x_k, w_k), & w_k &\sim N(0, R(k))
\end{aligned}
\tag{4.6}
$$

with input u_k, process noise v_k, measurement y_k and measurement noise w_k. The process and measurement noise are independent of each other, white and with normal probability distributions.

The objective of the filter is to estimate the state of the system based on the model and past measurements. The *a priori* state estimation $\hat{x}_k(-)$ and error

covariance $P_k(-)$ estimates are defined as

$$\hat{x}_k(-) = E[x_k|Y^{k-1}] \tag{4.7}$$
$$P_k(-) = E[(x_k - \hat{x}_k(-))(x_k - \hat{x}_k(-))^\top|Y^{k-1}] \tag{4.8}$$

where $Y^{k-1} = \begin{bmatrix} y_0 & y_1 & \dots & y_{k-1} \end{bmatrix}$ is a matrix containing the past measurements.

The *a posteriori* update of the state estimation $\hat{x}_k(+)$ is performed in the filter so that the error covariance is minimized. This results in the Kalman gain K_k

$$\hat{x}_k(+) = \hat{x}_k(-) + K_k[y_k - g(\hat{x}_k(-), w_k)] \tag{4.9}$$
$$K_k = P_{xy}(k)P_y^{-1}(k) \tag{4.10}$$

where

$$\hat{y}_k(-) = E[y_k|Y^{k-1}] \tag{4.11}$$
$$P_{xy}(k) = E[(x_k - \hat{x}_k(-))(y_k - \hat{y}_k(-))^\top|Y^{k-1}] \tag{4.12}$$
$$P_y(k) = E[(y_k - \hat{y}_k(-))(y_k - \hat{y}_k(-))^\top|Y^{k-1}]. \tag{4.13}$$

The corresponding *a posteriori* update of the covariance matrix $P_k(+)$ is

$$P_k(+) = E[(x_k - \hat{x}_k(+))(x_k - \hat{x}_k(+))^\top|Y^k] = P_k(-) - K_k P_y(k) K_k^\top. \tag{4.14}$$

Because for nonlinear systems calculation of the expectations is in most cases difficult, the state and output equations are approximated. A common way to do this is by Taylor approximations which results in the Extended Kalman filter, see eg. Gelb et al. (2001). Due to the approximation of the nonlinear equations the filter is no longer an optimal filter in the above mentioned sense.

For the estimation of the parameters of the metronomes a different extension of the linear Kalman filter is used. The filter proposed in Nørgaard et al. (2000), solves the problem of calculation of the expectations by making use of polynomial approximations and stochastic decoupling. In particular, a multidimensional extension of Stirling's interpolation formula is used which is introduced in appendix B. Secondly a linear transformation is used which performs a stochastic decoupling. For eg. state x_k this is done by calculating a Cholesky factor of the covariance P_x

$$P_x = S_x S_x^\top \tag{4.15}$$

so that the following applies for the transformed stochastic vector $z = S_x^{-1}x$

$$E[(z - E[z])(z - E[z])^\top] = I, \tag{4.16}$$

where I is the unity matrix.

The resulting equations to calculate the Kalman gain K_k and the *a priori* and *a posteriori* update of the covariance matrix P_k are given in appendix A and in more detail in Nørgaard et al. (2000).

The main advantage of the estimator is that the Jacobian of the state equations is no longer needed. Since the escapement is strongly nonlinear this makes implementation of the filter much easier.

Model of the metronome

The model which is used for the metronomes consists of the equations of motion in (3.9) without the terms relating to the translation of the platform. Secondly, the influence of the escapement is assumed to be asymmetric, i.e. different for negative and positive angles. This is expressed by an escapement forcing parameter ϵ^+ and escapement angles ϕ^+, $\Delta\phi^+$ for positive angles of the metronome and ϵ^-, ϕ^-, $\Delta\phi^-$ for negative angles. The equation of motion then becomes

$$\theta_i'' + \gamma_i^2 \sin\theta_i + \delta_i\theta_i' = \epsilon_i^+ \, \mathrm{f}(\theta_i, \theta_i') - \epsilon_i^- \, \mathrm{f}(-\theta_i, -\theta_i'). \tag{4.17}$$

where

$$\mathrm{f}(\theta, \theta') = \begin{cases} 0, & \theta < \phi \vee \theta > \phi + \Delta\phi \\ \frac{1 - \cos(2\pi\frac{\theta - \phi}{\Delta\phi})}{2\Delta\phi}, & \phi \leq \theta \leq \phi + \Delta\phi \wedge \theta' > 0 \end{cases} \tag{4.18}$$

Beside the angle θ and velocity θ', the following parameters will be estimated for each metronome: γ, δ, ϵ^+ and ϵ^-. The angles $\phi^{+,-}$ and $\Delta\phi^{+,-}$ will be chosen by hand as it turned out that the estimation of these angles did not converge.

In the filter the state $\hat{x}$ is defined as a concatenation of the original states and the parameters which need to be estimated

$$\hat{x} = \begin{bmatrix} \theta & \theta' & \gamma & \delta & \epsilon^+ & \epsilon^- \end{bmatrix}^\top. \tag{4.19}$$

Escapement angles

The angles ϕ and $\Delta\phi$ will not be estimated using the nonlinear filter but are chosen based on the plots in figure 4.4, where the velocity and acceleration are plotted versus the angle. The frequency of the metronomes is set to approximately 4 rad/s, almost three times as small as in the synchronization experiments. This is done to pronounce the effect of the escapement compared to the (viscous) damping in the system. The velocity and acceleration signal for the plot are obtained by numerically differentiating the angle. Before differentiation, the angle is filtered by a fourth order bandstop filter between 45 and 55 Hz to eliminate the disturbances around 50 Hz, without removing the signal at higher frequencies. In figure 4.3 the power spectral density is plotted for metronome I when oscillating with a constant amplitude.

In the plots the angles, between which the escapement is assumed to influence the pendulum, are indicated by dashed vertical lines. Although the escapement is modeled only as a single push, more complicated behavior can be seen. After the first increase of the velocity more oscillations are visible. These vibrations are probably caused by the fact that the next tooth of the escapement hits the other cam on the pendulum after the push. This effect is neglected, so the sinusoidal peak as described in (3.10) will be assumed to be an adequate model. The values of $\phi^{+,-}$ and $\Delta\phi^{+,-}$ are chosen by hand from figure 4.4 for metronome I and II and are given in rad below

$$\text{I:} \quad \phi^+ = 0.25, \quad \Delta\phi^+ = 0.07, \quad \phi^- = 0.24, \quad \Delta\phi^- = 0.06$$
$$\text{II:} \quad \phi^+ = 0.22, \quad \Delta\phi^+ = 0.09, \quad \phi^- = 0.28, \quad \Delta\phi^- = 0.06$$
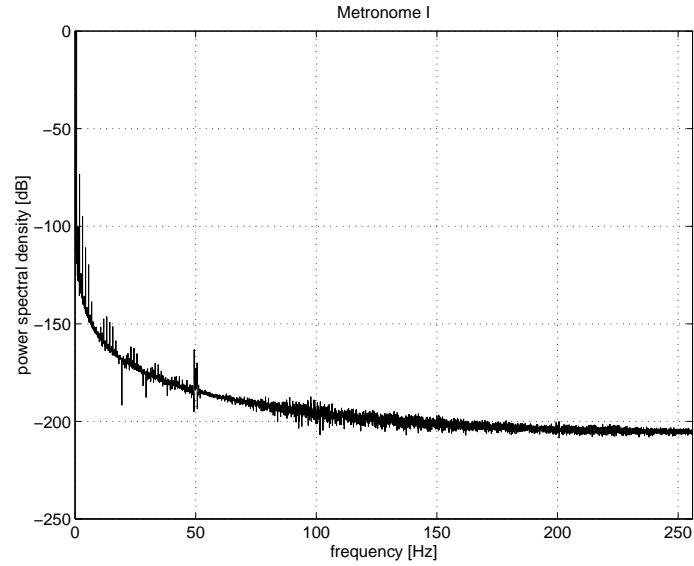
Figure 4.3: Power spectral density of a measurement of the angle of metronome I when oscillating with a constant amplitude.
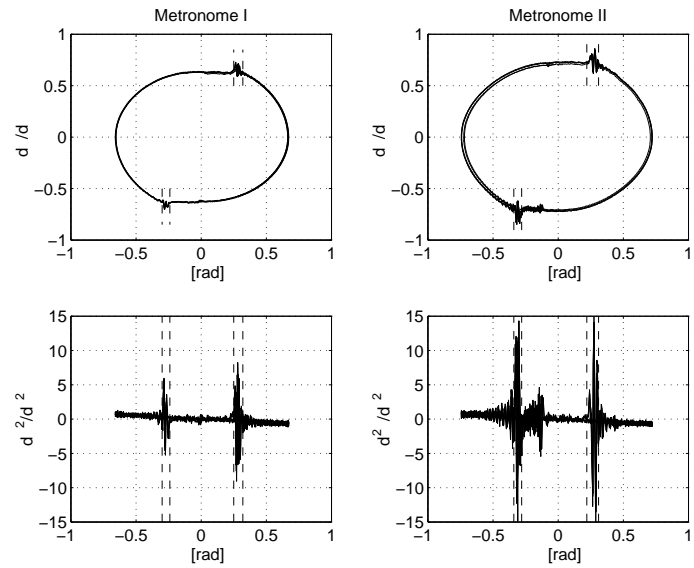

Figure 4.4: The velocity and acceleration are plotted versus the angle for both metronomes. The frequency of the metronome I and II is respectively 3.90 rad/s and 3.94 rad/s. Between the dashed vertical lines it is assumed, that the pendula receive a push from the escapement to increase the velocity of the pendulum.
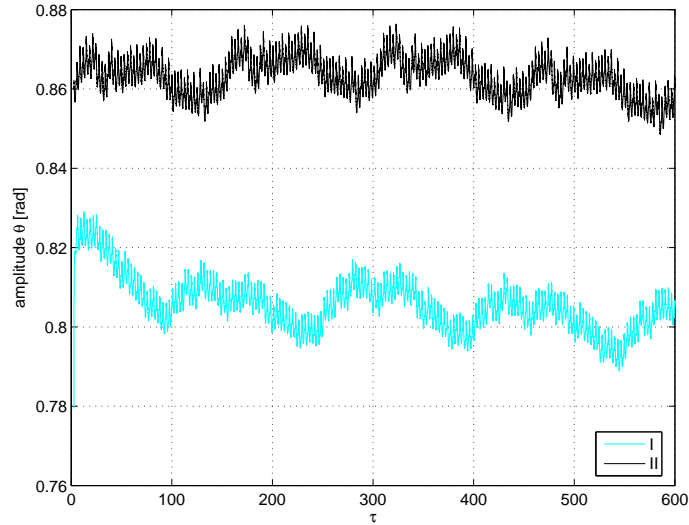
Figure 4.5: Amplitude of both metronomes in the experiment which is used for identification of the metronomes.

Parameter estimation

Given the angles between which the escapement operates, the states and other parameters can be estimated. With the platform held stationary the angles of the uncoupled oscillating metronomes are measured. When the metronomes oscillate with a steady amplitude, a measurement of one minute is performed. This corresponds to approximately a hundred oscillations. Using the Hilbert transform, see appendix C, the frequency of both metronomes is determined and given together with the mean frequency below in rad/s

$$\omega_1 = 10.565, \quad \omega_2 = 10.553, \quad \bar{\omega} = 10.559$$

Before filtering the data with the nonlinear estimator the time t in seconds is converted to the dimensionless time by $\tau = \bar{\omega}t$.

The amplitude of the oscillations is shown in figure 4.5. Between both metronomes a difference in amplitude is visible, which is probably caused by variation in manufacturing, for example in stiffness of the springs and friction in the joint. The amplitude of each metronome also shows a variation in time. This is probably due to the fact that the profile of the teeth, which transfers power from the spring of the escapement to the pendulum, differ from each other. In order to keep the model of the metronomes simple these variations are neglected however.

The initial conditions of the estimated state $\hat{x}$ are chosen in the following manner. First the measurements used in the filter are truncated in a smart way to obtain an estimate for the initial velocity of the pendulum. An extremum of the angle of the metronome is chosen as the first data point to be used in the filter. At this point the angular velocity is assumed to be zero. The initial condition for the first state, the angle, is then set equal to the measured angle and that

20

of the velocity of the pendulum to zero. The initial values of the parameters in $\hat{x}$ are chosen based on simulations which qualitatively give the same results as seen in the experiments and are for both metronomes:

$$\hat{\gamma}(0) = 1.0, \quad \hat{\delta}(0) = 0.02, \quad \hat{\epsilon}^+(0) = \hat{\epsilon}^-(0) = 0.05$$

The Kalman filter has to be initialized with the initial error covariance matrix P_0, process noise covariance Q and measurement noise covariance r. The values of these covariance matrices are chosen based on engineering insight and with fine-tuning by hand. The measurement noise covariance is set at a large value of $r = 1 \cdot 10^{-2}$ compared to the resolution of the angular measurement of $1 \cdot 10^{-3}$ rad. This value is estimated from variation of the measured angle when the metronomes are at rest. The large value of the measurement noise covariance appears to be necessary in order to estimate the parameters properly. For smaller values the parameters do not converge to a constant value but adapt due to the variation in amplitude of the metronome as seen in figure 4.5. Since these characteristics are not modeled, the noise covariance is increased to ignore the variation.

The process noise covariance is chosen as a diagonal matrix since no coupling between the elements of the estimated state $\hat{x}$ is assumed. The values are

$$Q = \begin{bmatrix} 1 \cdot 10^{-6} & 0 & 0 & 0 & 0 & 0 \\ 0 & 1 \cdot 10^{-3} & 0 & 0 & 0 & 0 \\ 0 & 0 & 1 \cdot 10^{-6} & 0 & 0 & 0 \\ 0 & 0 & 0 & 1 \cdot 10^{-6} & 0 & 0 \\ 0 & 0 & 0 & 0 & 1 \cdot 10^{-6} & 0 \\ 0 & 0 & 0 & 0 & 0 & 1 \cdot 10^{-6} \end{bmatrix}.$$

The first element of Q is chosen small since the relation between the angle and the velocity is assumed to be valid, the second value deals with the second time derivative of the angle. The covariance of this term is chosen large to accommodate for unmodeled forces acting on the metronome which show up in this part of the equation of motion. The process noise covariance of the parameters is set to a small but non-zero value since these parameters are assumed to be constant, but at the same time it is uncertain whether the model is correct. Finally for the initial error covariance matrix P_0 a diagonal matrix is chosen as

$$P_0 = \begin{bmatrix} 1 \cdot 10^{-2} & 0 & 0 & 0 & 0 & 0 \\ 0 & 1 \cdot 10^{0} & 0 & 0 & 0 & 0 \\ 0 & 0 & 1 \cdot 10^{-1} & 0 & 0 & 0 \\ 0 & 0 & 0 & 1 \cdot 10^{-1} & 0 & 0 \\ 0 & 0 & 0 & 0 & 1 \cdot 10^{-1} & 0 \\ 0 & 0 & 0 & 0 & 0 & 1 \cdot 10^{-1} \end{bmatrix}.$$

With these settings the states and parameters of both metronomes are estimated. In figure 4.6 the time series of the estimated parameters are plotted. The horizontal lines in the plot indicate the mean value and the standard deviation around the mean in the last half of the experiment. Within the duration of the experiment all parameters converge to a constant value. However a difference in convergence time and variation of the final value can be observed. The

Table 4.2: The mean values of the estimated parameters for metronomes I and II are given in this table, together with the standard deviation (std) around the mean. These values are calculated from the last half of the time series in order to exclude the transient behavior at the start of the filtering.

	run	γ		δ $[\cdot 10^{-2}]$		ϵ^+ $[\cdot 10^{-2}]$		ϵ^- $[\cdot 10^{-2}]$	
		mean	std	mean	std	mean	std	mean	std
I	1st	1.04462	$1.1 \cdot 10^{-4}$	2.374	0.020	4.795	0.031	5.180	0.033
I	2nd	1.04459	$1.2 \cdot 10^{-4}$	2.353	0.021	4.760	0.018	5.145	0.020
II	1st	1.04995	$1.1 \cdot 10^{-4}$	2.311	0.019	5.269	0.043	5.685	0.044
II	2nd	1.04993	$1.1 \cdot 10^{-4}$	2.295	0.018	5.235	0.023	5.653	0.030

parameters ϵ^+ and ϵ^- reach their final value the slowest. This can be explained by the fact that these parameters only have an influence on the system when the escapement acts on the pendula.

Using the final values of the parameters as initial conditions and the last value of the error covariance P for the initial covariance matrix P_0 the data is filtered again. The resulting time series of the parameters are plotted in figure 4.7. Here it can be seen that the parameters do not diverge from the initial values. This can also be seen in table 4.2 where the mean values and the standard deviation for the metronomes and both runs of the filter are given.

Verification

The model for the metronomes with the estimated parameters are compared to two different measurements. First a simulation is run with the same initial conditions as the experiments used for estimating both metronomes. The results are given in figure 4.8 where the amplitude of the oscillations is plotted together with the difference in phase of the simulated response and the measurement. In these plots it can be seen that the model matches the experiments qualitatively, but differences are present.

First of all, as expected, the amplitude of the oscillations in the simulations do not vary during time, this is due to the choice of the model of the escapement. The amplitude of the simulated response is on average also larger than the amplitude of the measured angles. This is most visible for metronome I, were the difference is about 1%. In the plot of the phase difference between the simulated and measured oscillation an increasing phase difference is visible. This means that the measurement has a slightly higher frequency than the simulated metronome. In one hundred oscillations this grows to approximately 0.7π rad, per oscillation a difference of about 0.4%. Although this is a small value, over time the simulated and measured response diverge, since the phase error accumulates.

In the second set of experiments, which are compared to simulations with the identified parameters, the initial angle of the pendula is smaller than the final amplitude of the oscillations. In figure 4.9 the amplitude and difference in phase of the experiments and simulations are plotted. For both metronomes the final amplitude reached in the simulation, matches the amplitude of the measurements, but the time in which this steady state is reached, is smaller.
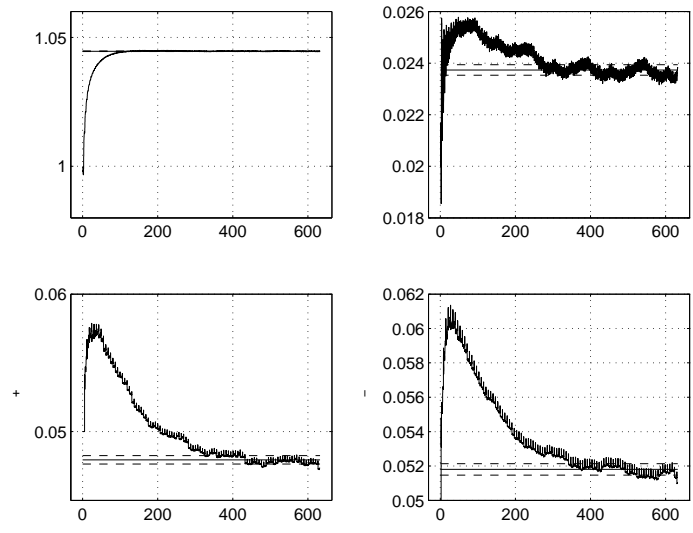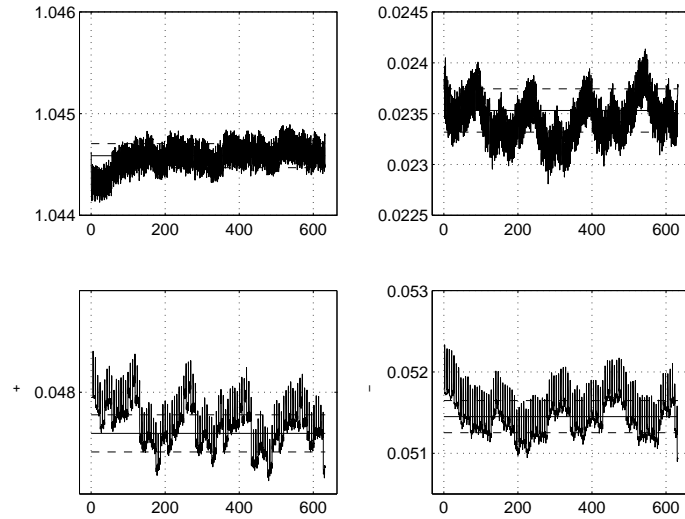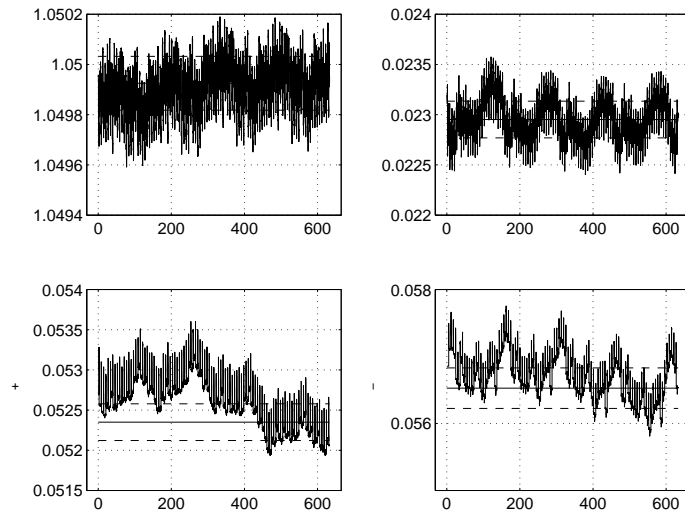
(a) Metronome I
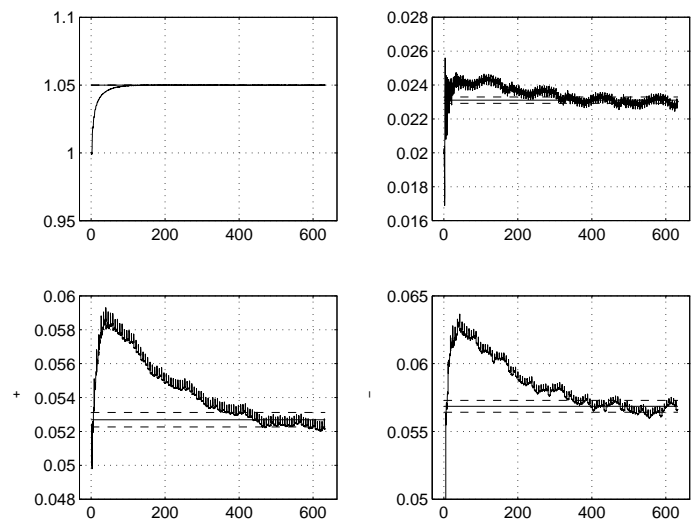
(b) Metronome II

Figure 4.6: Estimated parameters for metronome I and metronome II after a first run with the chosen settings and initial conditions of the filter. The horizontal line in the subplots indicates the mean value of the parameter over the last half of the experiment and the dashed lines the standard deviation around the mean.

(a) Metronome I

(b) Metronome II

Figure 4.7: Estimated parameters for metronome I and II with the resulting values of the first estimation as initial conditions. The error covariance matrix is initialized with the last values from P obtained in the first run. The horizontal solid line in the subplots indicates the mean value of the parameter over the last half of the experiment and the dashed lines the standard deviation around the mean of the interval.
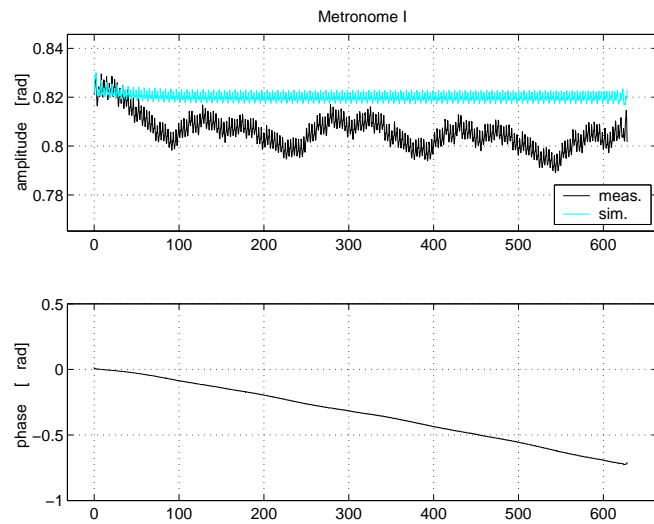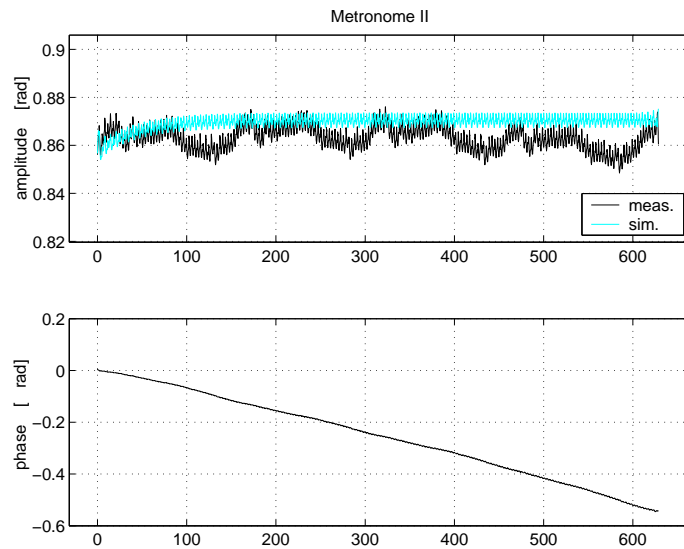
The phase difference between the measurement and simulation shows an error of about 1.2π rad over approximately 140 oscillations, a relative error of 0.4% per oscillation. This error in phase is comparable to the findings in the previous comparison between simulation and experiment in figure 4.8.

(a) Metronome I

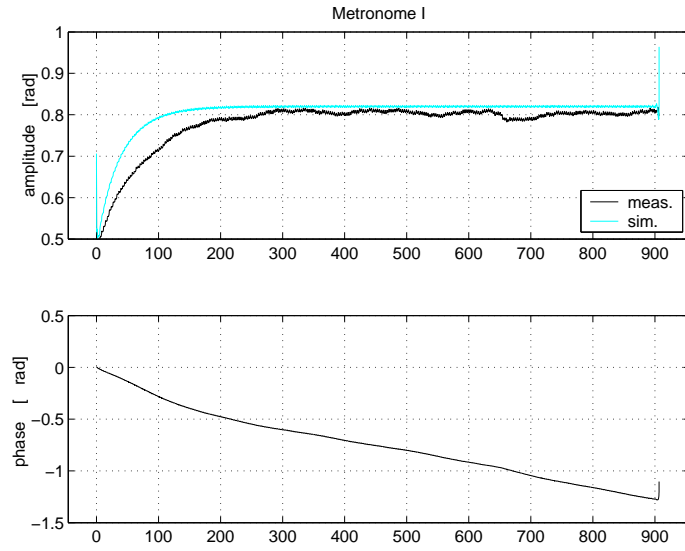(b) Metronome II

Figure 4.8: The measured angle of the metronomes is compared to simulations run with the estimated parameters. The amplitude of the oscillations is given in the upper plot of each subfigure, the difference in phase between the simulation and experiment in the lower subplot. A negative phase difference implies the simulated response oscillates slightly slower than the measurement.

(a) Metronome I
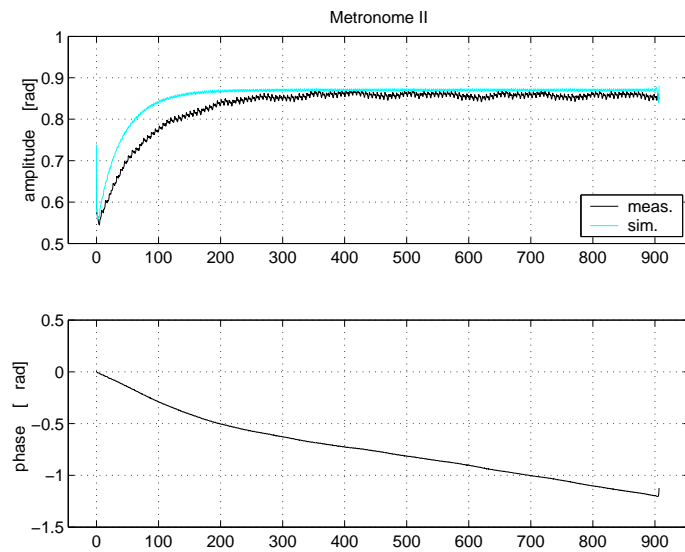
(b) Metronome II

Figure 4.9: The model simulated with the estimated parameters is compared to a different measurement. The metronomes are started from an angle smaller than the steady state amplitude that is reached. This is visible in the upper plot for each metronome where amplitude of the oscillations is given. The difference in phase between the simulation and experiment is plotted in the lower subplot. A negative phase difference implies the simulated response oscillates slightly slower than the measurement.

4.3 Coupling parameter

The only parameters that are not estimated yet, are the coupling parameters β_i, where i is 1 or 2 for either metronome I or II. This parameter determines how much influence a metronome has on the platform. In the derivation of the model the parameter is defined as the ratio between the mass of the pendulum m and the platform M. To verify whether the coupling parameter is inversely proportional to the mass of the platform, β is estimated for several values of M.

In order to keep the estimation as simple as possible, experiments are performed with one metronome fixed, while the other is oscillating on the platform. The equations of motion for this system are

$$\theta_i'' + \gamma_i^2 \cos\theta_i y'' + \gamma_i^2 \sin\theta_i + \delta_i\theta_i' = \epsilon_i \mathrm{f}_i \qquad (4.20)$$
$$y'' + 2\Omega\xi y' + \Omega^2 y + \beta_i\gamma_i^{-2}\big(\cos\theta_i\theta_i'' - \sin\theta_i\theta_i'^2\big) = 0,$$

where i is either 1 or 2 for metronome I and II.

The estimation is carried out with the same nonlinear Kalman filter used for finding the parameters of the metronomes. All parameters beside β_i are set to the values found in the previous estimations. The state $\hat{x}$ of the filter consists of the angle of the metronome θ, the position of the platform y, their time derivatives and the parameter β

$$\hat{x} = \begin{bmatrix} \theta & y & \theta' & y' & \beta \end{bmatrix}^\top \qquad (4.21)$$

The measurements which are used in the filter are the angle of the metronome and the position and velocity of the platform.

The process noise covariance matrix Q is set to

$$Q = \begin{bmatrix} 1\cdot 10^{-6} & 0 & 0 & 0 & 0 \\ 0 & 1\cdot 10^{-8} & 0 & 0 & 0 \\ 0 & 0 & 1\cdot 10^{-3} & 0 & 0 \\ 0 & 0 & 0 & 1\cdot 10^{-5} & 0 \\ 0 & 0 & 0 & 0 & 0 \end{bmatrix},$$

the initial proces noise covariance P_0 to

$$P_0 = \begin{bmatrix} 1\cdot 10^{-1} & 0 & 0 & 0 & 0 \\ 0 & 1\cdot 10^{-2} & 0 & 0 & 0 \\ 0 & 0 & 5\cdot 10^{-1} & 0 & 0 \\ 0 & 0 & 0 & 1\cdot 10^{-2} & 0 \\ 0 & 0 & 0 & 0 & 1\cdot 10^{-3} \end{bmatrix}$$

and the measurement noise covariance r to

$$r = \begin{bmatrix} 1\cdot 10^{-2} & 0 & 0 \\ 0 & 1\cdot 10^{-2} & 0 \\ 0 & 0 & 1\cdot 10^{-2} \end{bmatrix}$$

The initial conditions of the estimated states are set to the measured angle, position and velocity at $\tau = 0$. The measured data is clipped at a moment the angle of the metronome is maximal. The velocity of the metronome is assumed
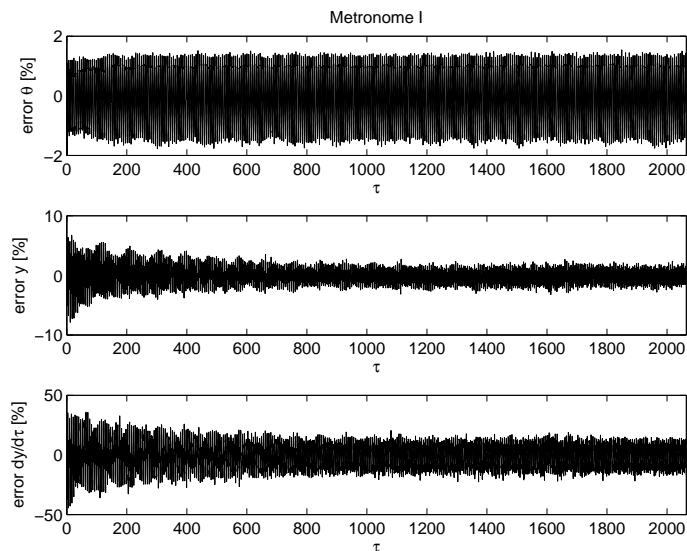
Figure 4.10: Error between measurements and estimated states plotted versus time. The resulting error is scaled with the amplitude of the corresponding state. The mass of the platform is 2.35 kg.

Table 4.3: For various mass of the platform the coupling parameter is given for metronome I (a) and II (b).

(a) Metronome I		(b) Metronome II	
M [kg]	$\beta\ [\times10^{-3}]$	M [kg]	$\beta\ [\times10^{-3}]$
2.35	3.77	2.35	3.86
3.75	2.34	3.75	2.38
5.17	1.70	5.17	1.69
6.78	1.29	6.78	1.27
8.18	1.06	8.18	1.03

to be zero at that moment. The initial guess for the parameter $\hat{\beta}$ is chosen based on simulations which are compared to the measurements.

In figure 4.10 the measurements of an experiment and the corresponding estimated states of the filter are plotted. A good match between the experiment and the filtered state can be seen. The time response of the estimated value $\hat{\beta}$ is given in figure 4.11. Here two runs of the filter are plotted, one with the initial covariance matrix P_0 and initial condition for $\hat{\beta}$ chosen as above, the second estimation is performed with the initial covariance matrix set to the values of the covariance matrix at the end of the first run. As can be seen the estimated value $\hat{\beta}$ is equal in both experiments when the value has converged.

The estimated values $\hat{\beta}$ for several masses of the platform are given in table 4.3 and are plotted in figure 4.12 versus $1/M$. A linear relation between the coupling parameter and the reciprocal mass can be seen for both metronomes. The values for each metronome differ from each other, but this is to be expected
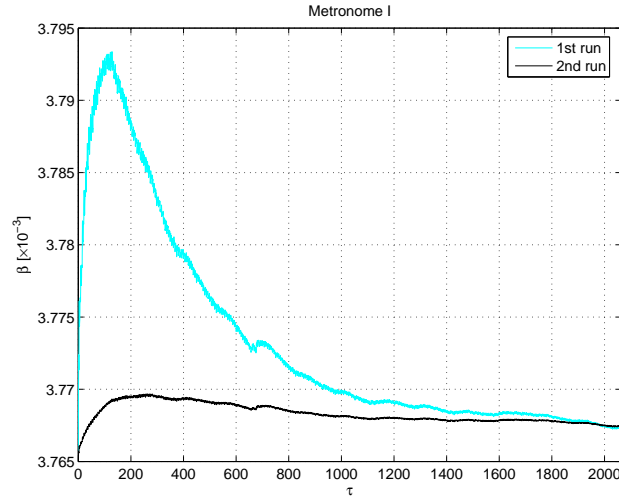
Figure 4.11: Estimated value of β versus time for to runs of the filter. In the first run the values of the initial covariance matrix P_0 and the initial condition for β are set to the described values. In the second run these values are set to the resulting covariance matrix P of the first run and the converged value of the estimated parameter β.

since the metronomes are not identical.

The obtained estimated value $\hat{\beta}$ is verified with an experiment by running a simulation with initial conditions equal to the experiment. In figure 4.13 the error between the simulation and measurement of the angle θ of metronome I, position y and velocity y' of the platform is plotted together with the simulated response. A good match between the measurement and the simulation can be seen. The results for different masses of the platform and metronome II are comparable.
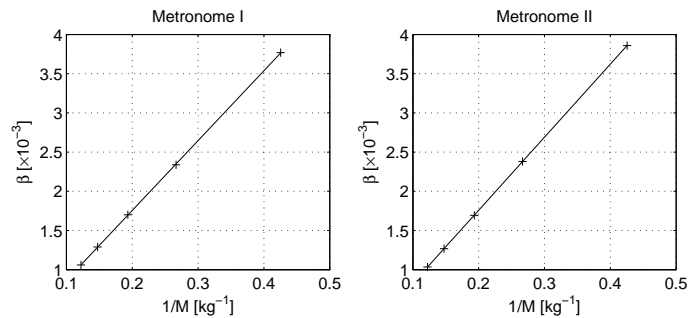
Figure 4.12: The estimated values of the coupling parameter β plotted versus the reciprocal mass of the platform. The results for both metronomes show a linear relation between β and $1/M$.
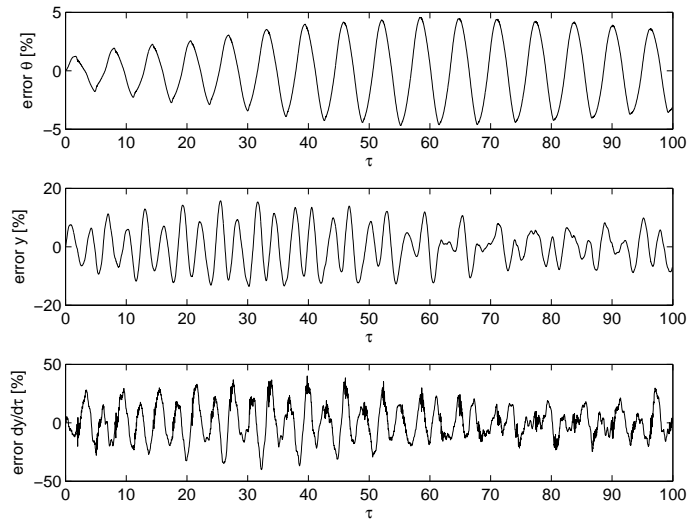
(a) Scaled error between measurement and simulation
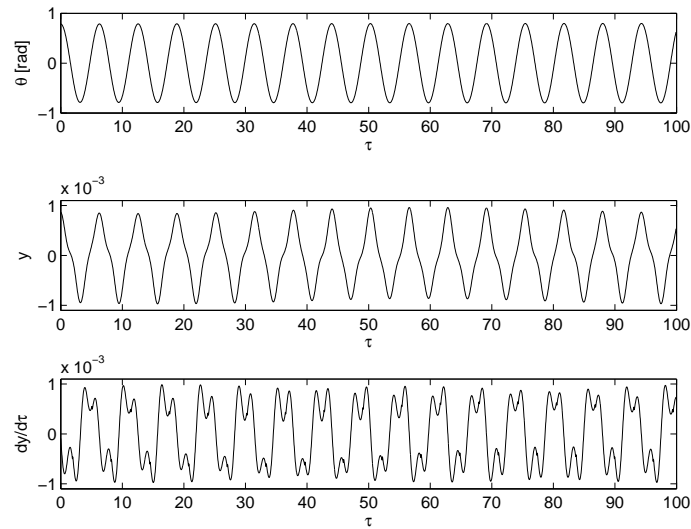
(b) Results simulation

Figure 4.13: In subfigure (a) the error between the simulated model with the estimated parameters and the measurements is plotted. The error signals are scaled with the maximal amplitude of the corresponding responses. The simulated response is plotted in subfigure (b). The mass of the platform is 2.35 kg in the experiment.

Chapter 5

Experiments

5.1 Anti-phase synchronization

Experiments have been performed with the setup to show synchronization of the metronomes. The parameters that can be varied in the experimental setup are the frequency of the metronomes and the mass of the platform.

The frequency of the metronomes is chosen as high as possible in order to reduce the time experiments will take. By adjusting the counterweights the frequency difference between both metronomes is minimized, since a too large difference will make synchronization impossible Bennett et al. (2002).

For anti-phase synchronization this can be explained as follows. If the metronomes have a nonidentical natural frequency and they would oscillate in exact anti-phase, the net force exerted by the two pendulums on the platform is not zero. For identical metronomes this force would be zero and due to the assumed damping of the leaf springs, oscillation of the platform damps out. However as there is still a net force from the metronomes, the platform will start to or keep oscillating. This translation of the platform will then disrupt the anti-phase oscillation of the metronomes. For increasing frequency difference of the metronomes, this is assumed to eventually lead to desynchronization.

Not only a difference in frequency between the metronomes will cause this effect. Also a difference in mass, damping or influence of the metronomes makes the metronomes nonidentical and prevents exact anti-phase synchronization.

The second parameter that can be changed is the mass of the platform. Changing this influences the dynamics of the system in three ways. First, the coupling between the metronomes changes since the coupling parameter β is proportional to the reciprocal mass of the platform. Secondly the relative eigenfrequency of the platform changes, increasing the mass of the platform lowers the eigenfrequency. Finally the relative damping factor of the platform depends on the mass, for increasing mass the dimensionless damping decreases.

Strong coupling

In the experiments the frequency of metronome I is set to 10.57 rad/s and that of metronome II to 10.55 rad/s, which results in a mean frequency of $\omega = 10.56$ rad/s and a relative frequency difference of 0.2%. The mass of the platform is varied between 2.35 kg and 8.18 kg in five steps, resulting in a coupling parameter β varying between $3.8 \cdot 10^{-3}$ and $1.1 \cdot 10^{-3}$. For each choice of mass the experiments are started with several initial conditions. Since the metronomes need to be started by hand, reproducing the initial conditions exactly between experiments is impossible.

When the mass of the platform is varied, the following observations can be made from the experiments. For small mass the setup synchronizes for seemingly all initial conditions and the difference in phase shows a variation of about 10%. When the mass of the platform increases the metronomes do not always synchronize anymore. When they do, the phase difference is comparable to that in experiments with small mass of the platform.

A typical example of the experiments, in which synchronization for seemingly all initial conditions is observed, is depicted in figure 5.1, where the difference in phase of the metronomes, their amplitudes and the dimensionless velocity of the platform are plotted. The mass of the platform in this experiment is 2.35 kg, resulting in a coupling factor $\beta = 3.8 \cdot 10^{-3}$, dimensionless eigenfrequency $\Omega = 2.1$ and dimensionless damping factor $\xi = 7.9 \cdot 10^{-4}$. The resulting difference in phase between the metronomes, when they are synchronized, is approximately 0.8π rad with a variation of 0.1π rad. The amplitude of the oscillations of metronome II is larger than that of metronome I, which is also the case, and with comparable magnitude, when the metronomes run uncoupled. The difference in amplitude of the metronomes is approximately 0.05 rad and the amplitude of metronome I and II is respectively about 0.82 and 0.87 rad.

The difference in amplitude might explain why the metronomes do not oscillate with a phase difference of π. Since the metronomes oscillate with different amplitudes when running uncoupled, they are nonidentical. As explained before no exact anti-phase synchronization is expected of nonidentical metronomes.

The variation in amplitude of the oscillations, which is also present when the metronomes run uncoupled, is probably the reason that the phase difference shows a large amount of variation.

Weak coupling

When the mass of the platform increases, the system does not synchronize for all initial conditions anymore. However some other interesting phenomena do occur. An example of such an experiment, is plotted in figure 5.2, where $M = 5.17$ kg and accordingly $\beta = 1.7 \cdot 10^{-3}$, $\Omega = 1.6$ and $\xi = 6.8 \cdot 10^{-4}$. After approximately $\tau = 2000$ the system looses synchrony and the amplitude of the metronomes start oscillating in a peculiar way. When the amplitude of metronome II increases, the amplitude of metronome I decreases. Energy seems to be exchanged between both metronomes at a time scale approximately $100\times$ larger than that of the metronomes. The oscillations of the platform die out when the difference in amplitude between the metronomes is maximal and at
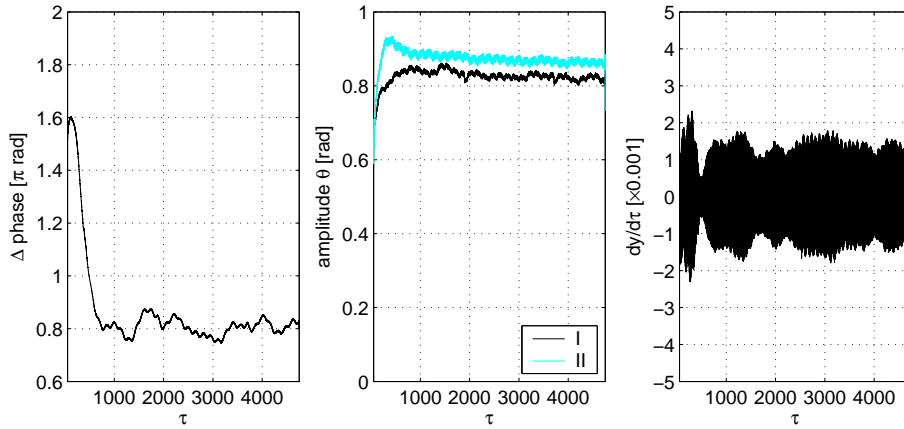
Figure 5.1: A synchronization experiment in which phase synchronization can be observed. The dimensionless parameters are as follows in the experiment, $\beta = 3.77 \cdot 10^{-3}$, $\Omega = 2.1$ and $\xi = 7.8 \cdot 10^{-4}$. The mean phase difference between both metronomes is 0.80π after $\tau = 1000$, but a variation of about 10% can be seen around this value.

about the same time the phase difference of the metronomes passes through an odd multiple of π. The system is thus momentarily in anti-phase synchronization but due to the large difference in amplitude of the metronomes this state is not stable.

A similar response can be seen in the experiment plotted in figure 5.3 with the same parameters as in the previous experiment, but with different initial conditions. Now the metronomes seem to synchronize around $\tau = 1000$, then diverge and synchronize again after $\tau = 2600$. However the length of the experiment is too short to be sure whether the metronomes will not desynchronize again. The increase and decrease of the amplitude of each metronome and quenching of the platform's oscillation is also present in this experiment.

In the performed experiments phase synchronization of two metronomes is visible, however the influence of disturbances in the system are clearly visible in the difference in phase of the metronomes. One of the disturbances acting on the system is the irregular operation of the escapement. Due to this the amplitude of the uncoupled metronomes also show a variation of about 10% when oscillating, as shown in figure 4.5.
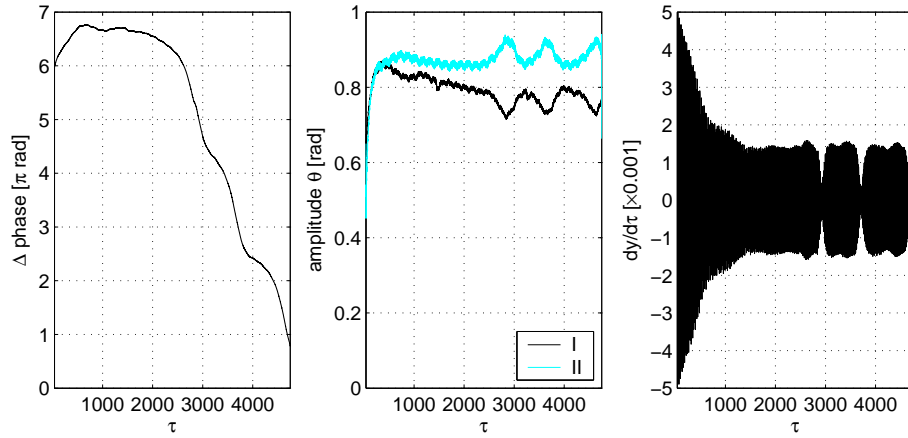
Figure 5.2: Experiment with $\beta = 1.7 \cdot 10^{-3}$ in which synchronization is lost. When this happens the amplitudes of the metronomes diverge and start oscillating. The parameters in this experiment are $\beta = 1.7 \cdot 10^{-3}$, $\Omega = 1.6$ and $\xi = 6.8 \cdot 10^{-4}$.
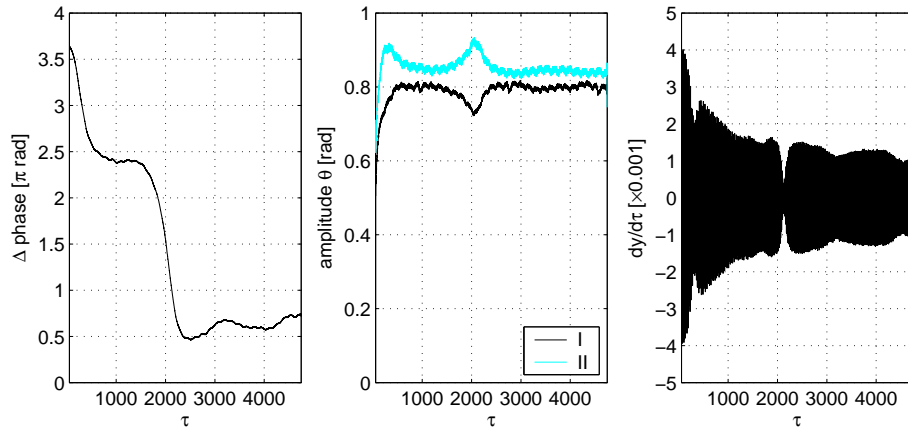
Figure 5.3: After losing synchronization around $\tau = 2000$ the system synchronizes again with a phase difference of 0.8π. The parameters in this experiment are $\beta = 1.7 \cdot 10^{-3}$, $\Omega = 1.6$ and $\xi = 6.8 \cdot 10^{-4}$.

5.2   In- and anti-phase synchronization

In a slightly changed experimental setup more types of synchronization can be observed. Instead of leaf springs of 0.4 mm thickness, more flexible leaf springs with 0.1 mm thickness are used. With this change in the experimental setup the value of Ω is approximately 1. A major drawback of this value is that resonance of the platform is possible since the frequency of the platform is close to that of the metronomes. When the oscillations of the platform become too large, the metronomes will hit the frame. To prevent this, damping of the platform is increased using magnetic damping. The extra damping also decreases the eigenfrequency of the platform, but this change is less than 1% for the current setup. The counterweights of the metronomes are removed in these experiments, as a result of which the frequency of the metronomes increases to 12.18 rad/s and the relative frequency difference to 1%, which is higher compared to the previous experiments.

For a small coupling parameter the system exhibits approximate anti-phase synchronization, as can be seen in figure 5.4. The mass of the platform is 2.35 kg in this experiment, resulting in a coupling strength $\beta = 9.6 \cdot 10^{-3}$, relative eigenfrequency $\Omega = 0.96$ and dimensionless damping $\xi = 7.8\%$. When the mass of the platform increases, anti-phase synchronization does no longer occur, instead the metronomes synchronize in two different ways depending on the initial conditions. In figure 5.5 in-phase synchronization is obtained after starting the metronomes with approximate equal angles. If the metronomes are started in anti-phase, the system synchronizes to a constant phase difference of about 0.67 and a large difference in amplitude between metronome I and II, which is shown in figure 5.6. In both figures the mass of the platform is 4.56 kg, resulting in a coupling strength $\beta = 4.7 \cdot 10^{-3}$, relative eigenfrequency $\Omega = 0.94$ and dimensionless damping $\xi = 4.2\%$.

A difference in amplitude of the platform's oscillations is visible between in- and anti-phase synchronization, in figure 5.4 and 5.5. When the metronomes oscillate with anti-phase synchronization, the amplitude of the velocity of the platform is about $0.7 \cdot 10^{-2}$, whereas the amplitude of the platform's velocity increases to $1.5 \cdot 10^{-2}$ when the metronomes show in-phase synchronization. For perfect anti-phase synchronization one would expect the platform to stop oscillating as the net force from both metronomes on the platform is zero. However in the experiment, due to differences between the metronomes, the phase differences with which the metronomes synchronize is not exactly π rad and the amplitudes of the metronomes are not equal. As a result the metronomes still excite the platform. In the case of in-phase synchronization the force of the metronomes acting on the platform is combined instead of canceled and a larger amplitude of the platform's oscillation can be expected.
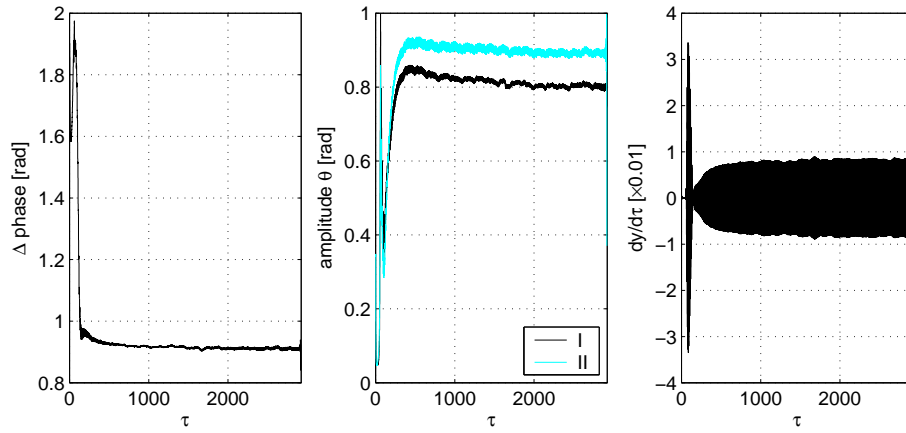
Figure 5.4: Experiment in which the metronomes synchronize with approximate anti-phase. The parameters of the system are $\beta = 9.6 \cdot 10^{-3}$, $\Omega = 0.96$ and $\xi = 7.8 \cdot 10^{-2}$.
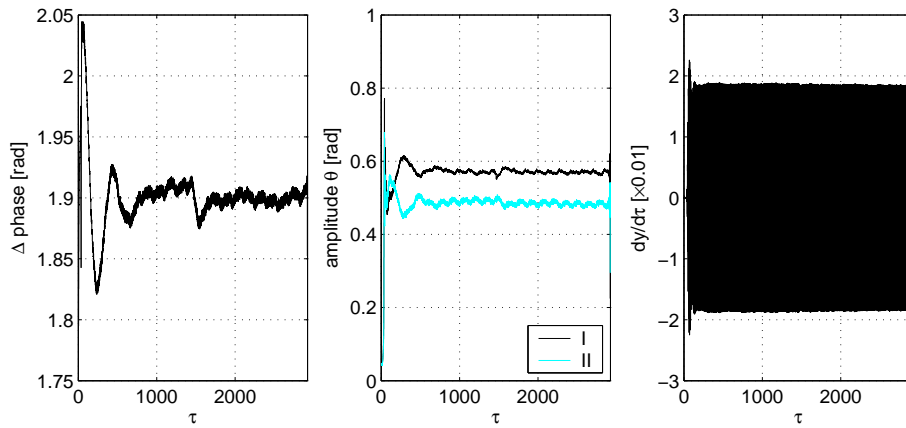
Figure 5.5: For large enough mass of the platform and with the initial conditions close to in-phase synchronization, the metronomes synchronize in-phase. The parameters of the system are $\beta = 4.7 \cdot 10^{-3}$, $\Omega = 0.94$ and $\xi = 4.2 \cdot 10^{-2}$.

Figure 5.6: The metronomes synchronize with a constant phase but a large difference in amplitude for equal parameters of the system as when in-phase synchronization is observed, the initial conditions differ however. The parameters of the system are $\beta = 4.7 \cdot 10^{-3}$, $\Omega = 0.94$ and $\xi = 4.2 \cdot 10^{-2}$.

Chapter 6

Simulations

Simulations with the model proposed in chapter 3 and estimated parameters from chapter 4, have been performed and are compared to the results obtained in the experiments.

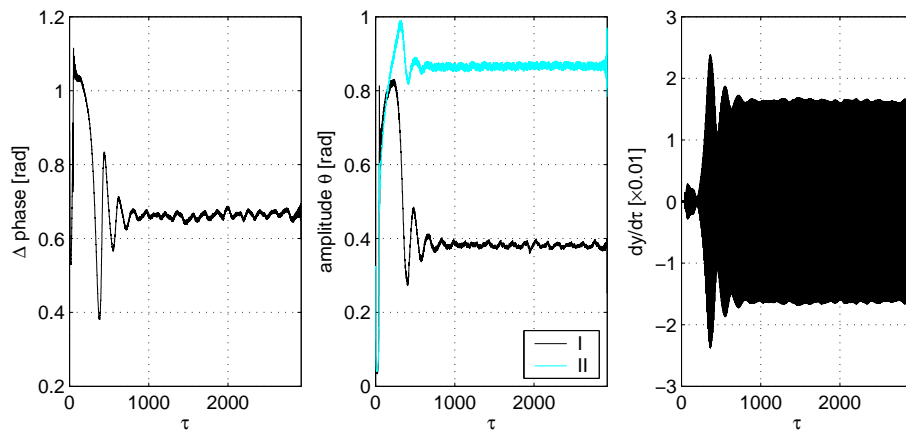## 6.1 Anti-phase synchronization

The values of the parameters of the metronomes used in the simulations are given in table 6.1. The other parameters are given for each individual comparison between experiment and simulation as they depend on the chosen mass of the platform.

Strong coupling

In figure 6.1 a simulation is compared to the experiment, in which anti-phase synchronization is observed. In general, matching dynamics can be seen, but differences are present as well. First of all the metronomes do synchronize in approximate anti-phase style, but not with the same phase difference as in the experiment. Whereas the real metronomes have a phase difference of approximately 0.8π rad, in the simulation it is 0.95π rad. Apparently the model approaches exact anti-phase synchronization more closely than the real metronomes do. This also effects the oscillation of the platform, its velocity is

Table 6.1: Values of the parameters of the metronomes I and II.

| (a) Metronome I				(b) Metronome II			
			[rad]				[rad]
γ	1.0446	ϕ^+	0.25	γ	1.0499	ϕ^+	0.22
δ	$2.35 \cdot 10^{-2}$	ϕ^-	0.24	δ	$2.30 \cdot 10^{-2}$	ϕ^-	0.28
ϵ^+	$4.76 \cdot 10^{-2}$	$\Delta\phi^+$	0.07	ϵ^+	$5.24 \cdot 10^{-2}$	$\Delta\phi^+$	0.09
ϵ^-	$5.15 \cdot 10^{-2}$	$\Delta\phi^-$	0.06	ϵ^-	$5.65 \cdot 10^{-2}$	$\Delta\phi^-$	0.06

about four times smaller in the simulation compared to the experiment. The amplitudes of the metronomes show the same behavior and magnitude in the simulation as in the experiment, a difference between the amplitudes remains after the system has synchronized.

The steady state response of the simulation and experiment are plotted for a few oscillations in figure 6.2. Now the behavior of the metronomes and platform is visible in more detail. In order to compare the responses more easily the time window is different for the experiment and simulation, but with approximate equal phase for metronome I at the beginning. In these plots the difference between the simulated and measured amplitude of the platform can be seen. The amplitude differs about a factor four, but the shape of the oscillation is comparable. In the response of the platform, the influence of the metronomes and the eigenfrequency of the platform, which is exactly twice as high as the frequency of the metronomes, can be seen.

The frequency difference between the metronomes seems to be a key factor in the dynamics of the setup. After adjusting the parameter γ_2, which regulates the frequency of metronome II, from the estimated value of 1.0499 to 1.0488, the response of the simulated systems matches the experiment almost perfectly. In figure 6.3 the phase difference, amplitude of the metronomes and the velocity of the platform is plotted. Here it can be seen that the phase difference is approximately 0.8π rad after synchronization, which is also observed in the experiment. The velocity of the platform also shows a better match compared to the previous simulation. Apparently the resulting oscillation of the platform is mainly dictated by the phase difference between the metronomes when the system has synchronized.

The reason why changing the value of γ_2 gives better results, can be explained by comparing the frequency difference between the two metronomes in both experiments and in simulations. In figure 6.4 the phase difference between the response of the uncoupled metronomes is plotted. A horizontal line in this plot would mean that the metronomes run at exactly equal frequencies. It can be seen that the simulation with the adjusted value for γ_2 shows roughly the same response as the experiment, metronome I is oscillating slightly faster than metronome II. The other simulation, with the estimated value for $\gamma_2 = 1.0499$, has an opposite frequency difference, which is also smaller as the slope is less steep.

A thing that is still different between the simulation and the experiment is the time needed for synchronization, which is visualized in figure 6.5, where the phase difference between the metronomes of both the experiment and the two simulations are plotted. Here it can be seen that the slope of the phase difference is steeper in the experiment than in both simulations. The reason why this happens is unclear.
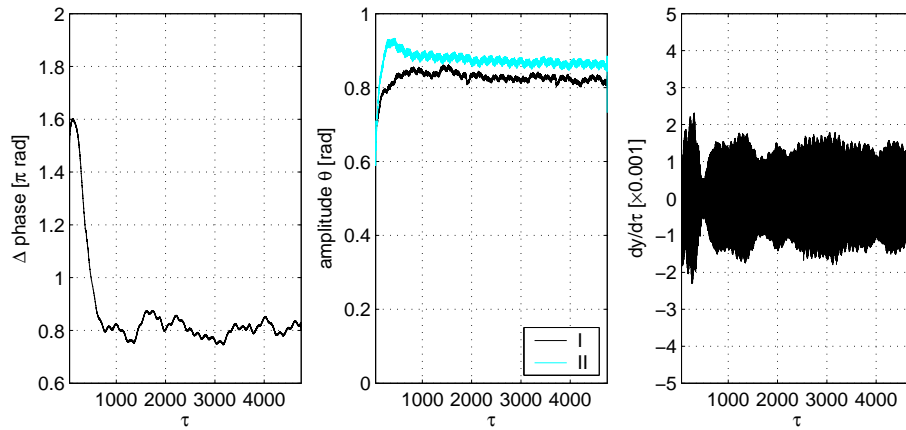
(a) experimental results
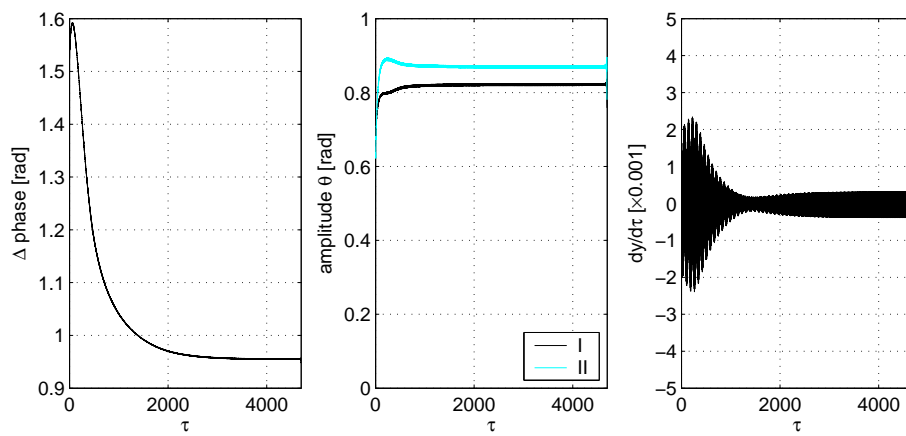
(b) simulation

Figure 6.1: Experimental results (a) and simulation (b) in which approximate anti-phase synchronization can be seen. The parameters of the system are $\beta = 3.77 \cdot 10^{-3}$, $\Omega = 2.1$ and $\xi = 7.8 \cdot 10^{-4}$.
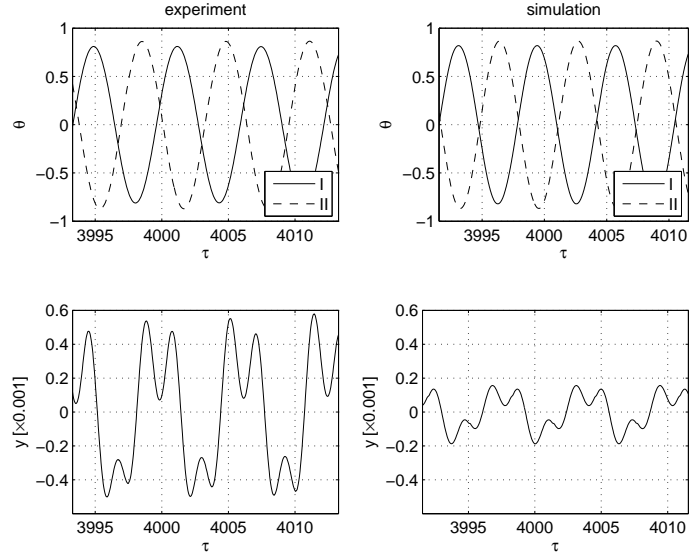
Figure 6.2: Steady state response of the experimental and simulated system, which shows approximate anti-phase synchronization. The angles of metronome I and II are given in the upper plots, the translation of the platform in the lower.

Figure 6.3: Simulation of the system with a slightly changed parameter γ_2 from the value which is estimated. Due to this changes the frequency difference between both metronomes decreases and better match with the experiment results. The parameters of the system are $\beta = 3.77 \cdot 10^{-3}$, $\Omega = 2.1$ and $\xi = 7.8 \cdot 10^{-4}$.
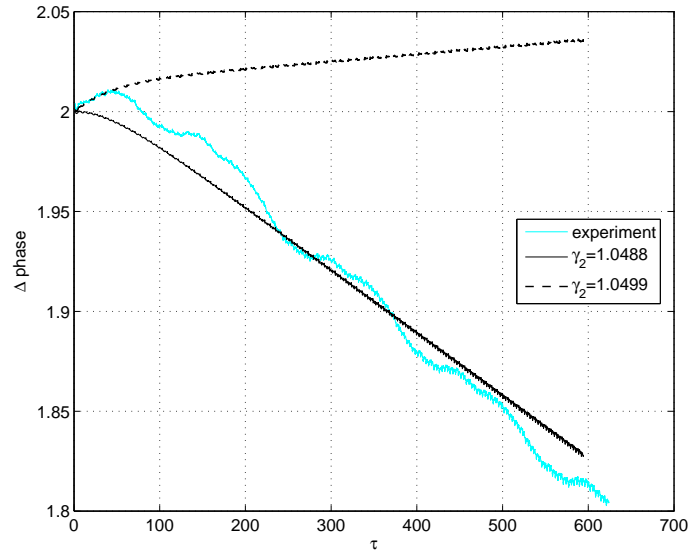
Figure 6.4: Phase difference between metronome I and II for different values of the parameter γ_2 and an experiment. The metronomes are running uncoupled in the experiment and simulations. A horizontal line in the plot would mean that the metronomes run at equal frequencies.
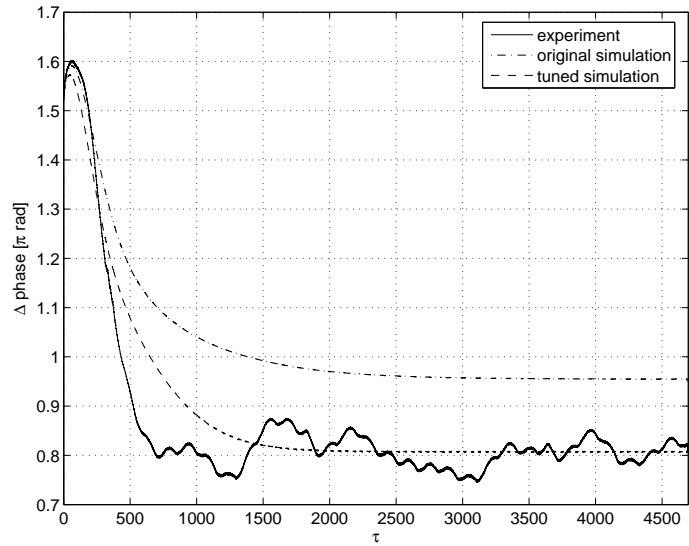
Figure 6.5: Phase difference between the metronomes for the experiment and two different simulations performed. The parameters of the first simulation are all directly estimated. In the second simulation the value for the parameter γ_2 is changed, which decreases the frequency difference between the metronomes. The parameters of the system are $\beta = 3.77 \cdot 10^{-3}$, $\Omega = 2.1$ and $\xi = 7.8 \cdot 10^{-4}$.

43

Weak coupling

In experiments with a larger mass of the platform, which results in a smaller coupling parameter and a lower eigenfrequency of the platform, the system does not synchronize for all initial conditions as shown in section 5.1. The experiment in which the system desynchronizes is compared with a simulation in figure 6.6. Here quite a different response can be seen, whereas the system does not synchronize in the experiment, the metronomes do synchronize in almost perfect anti-phase in the simulation. The remarkable increase and decrease in amplitude of the metronomes does not occur either. As expected the oscillations of the platform are relatively small since the metronomes almost reach anti-phase synchronization.

As for the experiment with anti-phase synchronization the parameter γ_2 is varied from its estimated value of 1.0499. In figure 6.7 a simulation with $\gamma_2 = 1.0464$ is plotted. Although the response is not equal to what is observed in the experiment, synchronization for a short while and after that desynchronization with the oscillations in the amplitude of the metronomes, this last effect is present in the simulation. A reason for the fact that only desynchronization can be seen in this simulation might be that the differences between the metronomes are too large, preventing synchronization. In the experiment the differences are possibly smaller, which makes synchronization possible, but due to the disturbances acting on the metronomes the system is pushed out of synchronization.

6.2   In- and anti-phase synchronization

The experiments, shown in section 5.2, with the thin leaf springs and a eigenfrequency of the platform of approximately $\Omega = 1$, are compared to simulations in this section.

The values of the parameters of the metronomes used in these simulations are given in table 6.2. The other parameters are given for each individual comparison between experiment and simulation as they depend on the chosen mass of the platform.

In figure 6.8 a simulation is shown with the same parameters and initial conditions as the experiment in which approximate anti-phase synchronization is observed. Qualitatively the same response can be seen, the metronomes have a phase difference of about 0.9π and the amplitude of metronome II is larger

Table 6.2: Values of the parameters of the metronomes I and II.

(a) Metronome I				(b) Metronome II			
			[rad]				[rad]
γ	1.0568	ϕ^+	0.25	γ	1.0549	ϕ^+	0.22
δ	$8.97 \cdot 10^{-3}$	ϕ^-	0.24	δ	$1.30 \cdot 10^{-2}$	ϕ^-	0.28
ϵ^+	$8.38 \cdot 10^{-3}$	$\Delta\phi^+$	0.07	ϵ^+	$3.20 \cdot 10^{-2}$	$\Delta\phi^+$	0.09
ϵ^-	$4.43 \cdot 10^{-2}$	$\Delta\phi^-$	0.06	ϵ^-	$3.05 \cdot 10^{-2}$	$\Delta\phi^-$	0.06

(a) experimental results
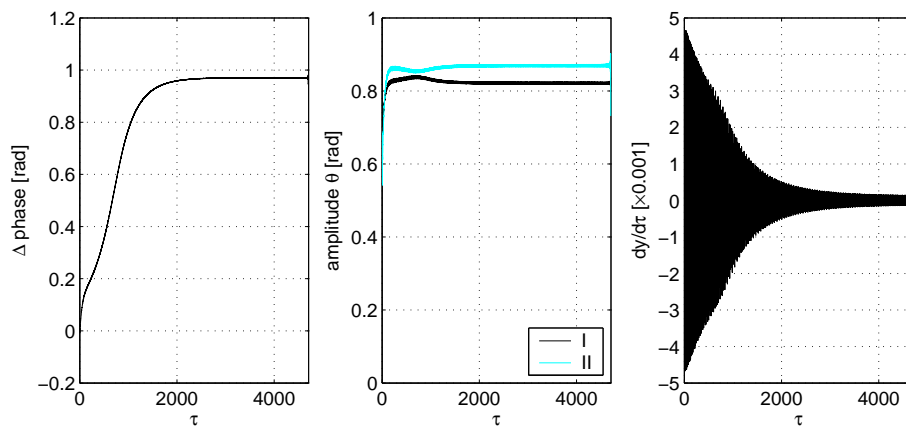
(b) simulation

Figure 6.6: Experimental results (a) and simulation (b) in which approximate anti-phase synchronization can be seen. The parameters of the system are $\beta = 1.7 \cdot 10^{-3}$, $\Omega = 1.6$ and $\xi = 6.8 \cdot 10^{-4}$.
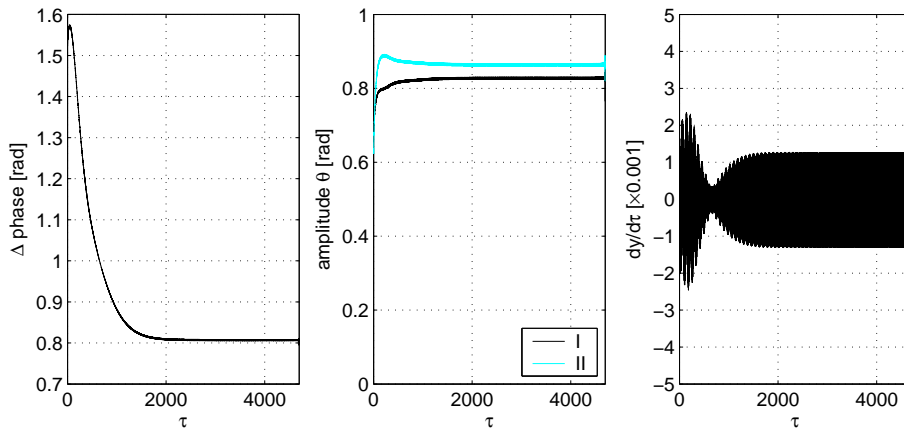
Figure 6.7: Simulation of the system with a slightly changed parameter γ_2 from the value which is estimated. Due to this changes the frequency difference between both metronomes decreases and better match with the experiment results. The parameters of the system are $\beta = 1.7 \cdot 10^{-3}$, $\Omega = 1.6$ and $\xi = 6.8 \cdot 10^{-4}$.

than that of metronome I, however differences between the experiment and the simulation can be seen. The velocity of the platform is approximately twice as large in the simulation compared to the experiment and the transient behavior differs quite. This can be seen in more detail in figure 6.9 where the angles and velocity of the platform are plotted versus time for both the simulation and the experiment. Whereas the angles of the metronomes have approximately equally increasing amplitudes in the experiment, a decrease in the amplitude of metronome II can be seen in the simulation around $\tau = 35$. This affects the oscillation of the platform as well, in the experiment the platform comes almost to a standstill around $\tau = 70$ whereas the platform does not slow down that much in the simulation.

The reason for this large difference in transient behavior remains unclear. The model of the escapement probably has influence, as the amplitude of metronome II decreases in the experiment as well, but does not become smaller than 0.3 rad, which is assumed to be the approximate angle at which the escapement stops working.

A simulation with the same parameters and initial conditions as an experiment in which in-phase synchronization is observed, is given in figure 6.10. The response of the model matches that of the physical setup, the metronomes synchronize in-phase, have a small difference in amplitude and the velocity of the platform is approximately equal. For different initial conditions, but equal parameters, the experimental setup also shows a type of synchronization where the phase difference between the metronomes is about 0.7π rad and the amplitudes of the metronomes differ a factor two. In simulations this response is found as well and is shown in figure 6.11. The role of the metronomes is switched however, in the simulation metronome I has the larger amplitude. Although not shown in this report this switch of role is also seen in experiments.

46
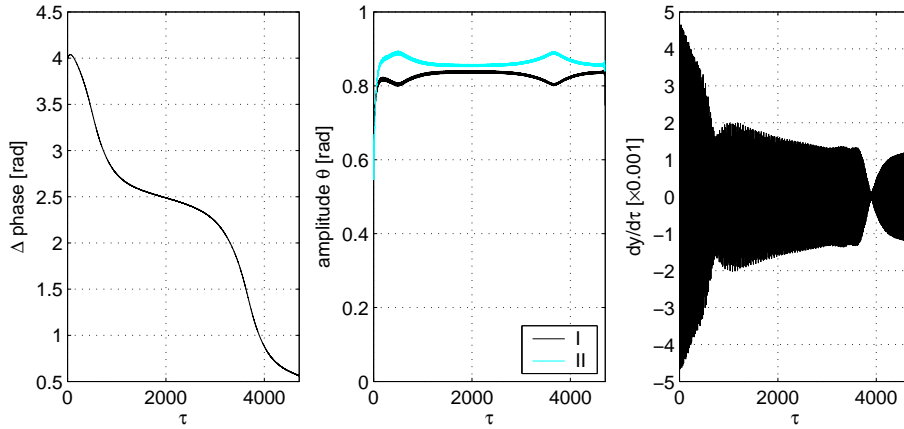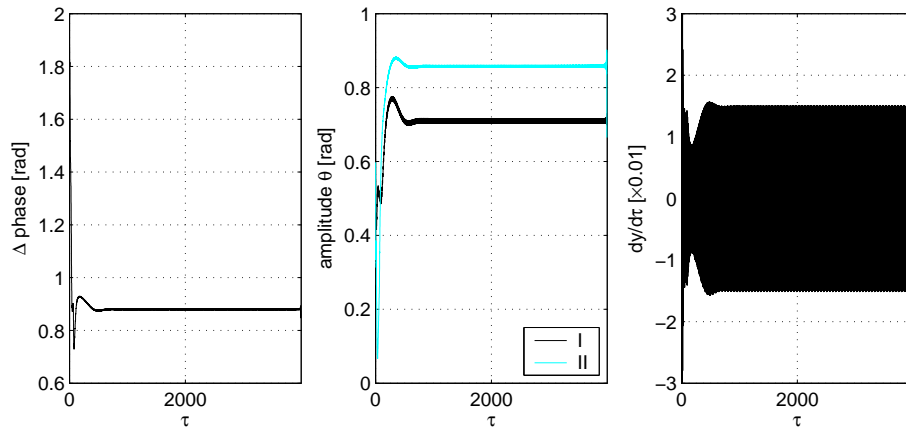
Figure 6.8: Simulation with the same parameters and initial conditions as the experiment in which anti-phase synchronization is observed. The parameters of the system are $\beta = 9.6 \cdot 10^{-3}$, $\Omega = 0.96$ and $\xi = 7.8 \cdot 10^{-2}$.
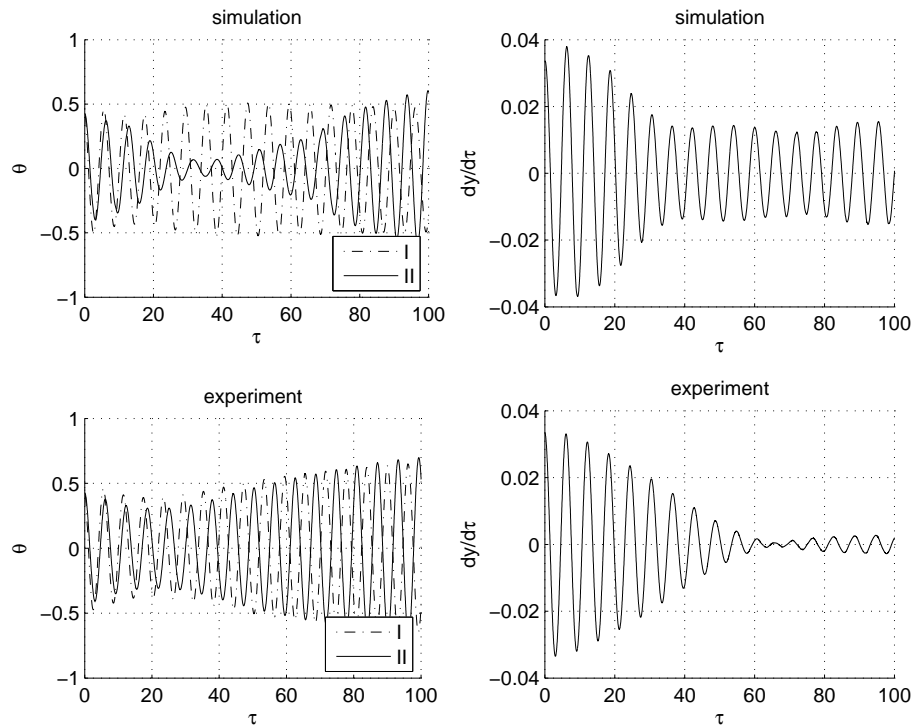
Figure 6.9: The transient of the angles of the metronomes and velocity of the platform are plotted for both the simulation and experiment. Around $\tau = 35$ a decrease in the amplitude of metronome II can be seen in the simulation, whereas this does not occur in the experiment. The parameters of the system are $\beta = 9.6 \cdot 10^{-3}$, $\Omega = 0.96$ and $\xi = 7.8 \cdot 10^{-2}$.
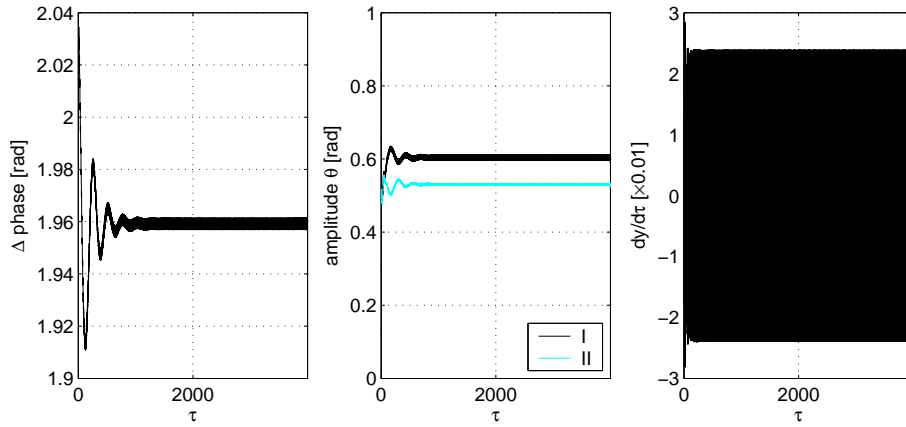
Figure 6.10: In-phase synchronization can be observed in this simulation. The parameters of the system are $\beta = 4.7 \cdot 10^{-3}$, $\Omega = 0.94$ and $\xi = 4.2 \cdot 10^{-2}$.
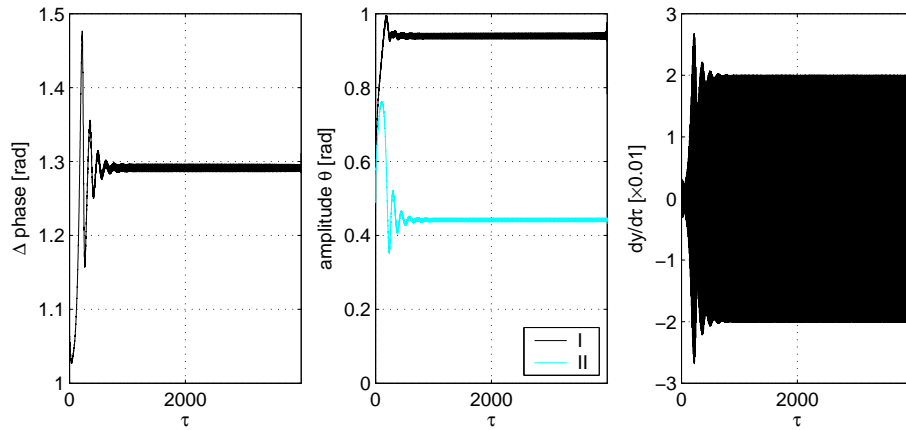
Figure 6.11: A simulation is shown where the metronomes synchronize with a phase difference of 1.3π rad and have a large difference in amplitude. The role of the metronomes is switched, compared to the response observed in a similar experiment. The parameters of the system are $\beta = 4.7 \cdot 10^{-3}$, $\Omega = 0.94$ and $\xi = 4.2 \cdot 10^{-2}$.

Chapter 7

Conclusions and recommendations

The objective of this research was to design an experimental setup in which synchronization of metronomes can be observed, perform experiments with the setup and verify the results with simulations. In order to keep the design simple, two off-the-shelf metronomes have been used as oscillators. Coupling between the metronomes is made possible by allowing horizontal translation of a platform on which they are mounted. To be able to study the dynamics, measurement of the angles of the metronomes and oscillation of the platform is made possible.

After designing and realizing the setup, experiments have been performed in which synchronization of the pendula is observed. In experiments with an eigenfrequency of the platform higher than the frequency of the metronomes, only anti-phase synchronization or no synchronization is obtained. In a slightly changed setup, where this eigenfrequency is approximately equal to the frequency of the metronomes, besides anti-phase synchronization also in-phase synchronization is observed.

In order to compare the experiments with simulations a model is proposed and the introduced parameters are estimated from experiments. The estimation is performed in three steps, first the parameters of the separate metronomes are identified, secondly the parameters of the platform without the oscillating metronomes are obtained and finally the coupling between each metronome and the platform is estimated. Using the model and these parameters, the results found in the experiments are compared to simulations.

In the following sections the conclusions and recommendations, which can be drawn from the presented work, will be given. Beside the discussion on the synchronization itself, extra attention is given to the practical implementation.

7.1 Conclusions

Experimental setup

An experimental setup, based on two off-the-shelf metronomes, has been realized. The use of leaf springs to suspend and allow only horizontal translation of the platform was successful. The chosen range of eigenfrequencies of the platform, which depends on the length and thickness of the leaf springs and the mass of the platform, was adequate for the synchronization experiments. In measurements the response of the platform showed linear spring stiffness and linear viscous damping for the amount of translation that is found in the synchronization experiments.

The chosen measurement system of the angle of the metronomes, using the magnetoresistance principle, performs well. The magnets which are needed, can be installed easily on the metronomes. Initial problems with nonlinear damping of the platform due to the electrical wires needed for the magnetic sensors have been solved by using thinner wires and a smarter routing. Measurement of the position and velocity of the platform was successful with the LASER vibrometer.

Although synchronization has been obtained with the metronomes, they are not ideal for experiments where the focus is on analysis of synchronization. The only thing that can be adjusted in the metronomes is their frequency. The amplitude cannot be changed, which is not ideal as the amplitude is rather large in the current setup. In some experiments this has proven to be a problem as the pendulum hits the supporting frame. Since these impacts are not modeled, they should be avoided. A final drawback of using the metronomes in the setup is the amount of variation they show in amplitude over a timescale of several oscillations.

Modeling and estimation

A model is derived to compare simulations with the experiments. The platform is modeled as a mass attached to the fixed world by linear springs and damping. The metronomes are modeled as pendula with a viscous damping term and a driving mechanism. Modeling this escapement proved to be the most difficult part. Based on measurements of a freely oscillating metronome, the escapement has been modeled as a sinusoid shaped pulse located between fixed angles, which gives the pendulum a push when moving upward. Besides the fact that it is only a crude approximation for the real dynamics present, it captures the essentials of the escapement. A disadvantage of the used model for the escapement is, that it is too complicated to be used analytically. This is be a problem for future research.

In order to make the model more transparent, it is made dimensionless by scaling time and introducing new parameters. The result of this transformation is that the influence of the dimensionless parameters is easier to understand, but a drawback is that a change of one of the physical parameters influences many dimensionless parameters.

The parameters defined in the model are estimated in three steps. First only the parameters of the platform are estimated, secondly the metronomes are

identified when oscillating freely and finally the coupling strength between the metronomes and the platform is estimated. By breaking up the complete model in smaller parts a better overview over the estimation is kept. For the identification a nonlinear Kalman filter is used, which uses interpolation to linearize the state equation. This filter is used since its implementation is simpler compared to a more common extended Kalman filter. According to the literature (Nørgaard et al. 2000), the filter should perform in practice at least as good as the extended Kalman filter, this is however not verified in this report.

When comparing the response of the subsystems to measurements, a good match is obtained. The largest differences are found in the response of the metronomes, which is not surprising as the model of the escapement is a crude approximation of a complex mechanism in reality.

The use of the Hilbert transform to calculate the phase and amplitude of the response of the metronomes gives good results. These properties of the signals characterize the dynamics of the system better than the angles itself. Although not a problem for this research, a drawback of the method is that it can only be used offline.

Experiments

Synchronization of the metronomes has been obtained with the experimental setup. Depending on the initial conditions and parameters of the system the metronomes synchronize with varying phase differences. Two distinct configurations, regarding the eigenfrequency of the platform relative to the frequency of the metronomes, have been studied.

When the pendula oscillate at a frequency lower than the resonance frequency of the platform, only anti-phase or desynchronization of the metronomes is observed. Whether and to what phase difference the system synchronizes seems to depend mainly on the coupling strength of the metronomes, the frequency difference between the metronomes and the initial conditions. For a relatively large coupling parameter the setup shows an approximate anti-phase synchronization for seemingly all initial conditions. The fact that the system does not oscillate in exact anti-phase and with equal amplitudes can be explained by the fact that the metronomes are nonidentical.

A mix of approximate anti-phase synchronization, no synchronization at all or desynchronization is observed when the coupling strength is decreased. What type of response is observed, is influenced by the initial conditions of the setup and by disturbances acting on the metronomes. Due to variation in the escapement mechanism which drives the pendula, the amplitude of the oscillations changes during time. Combined with the weaker coupling synchronization is sometimes lost or not obtained at all in the experiments. However if the metronomes do synchronize, it is in approximate anti-phase. The desynchronization which is observed, is attributed to the disturbances acting on the metronomes.

A richer set of responses is observed when the eigenfrequency of the platform is lowered to approximately the frequency of the metronomes by fitting thinner leaf springs. For this configuration anti-phase synchronization is observed for

strong coupling of the platform. But for a smaller coupling strength and a smaller relative eigenfrequency of the platform either in-phase synchronization or a response is found, where the phase difference between the metronomes is approximately 0.7π rad and a large difference between the amplitude of the metronomes exists.

Simulations

With the derived model and estimated parameters simulations have been performed and compared to the results found in experiments. A qualitative match is found between the simulations and experiments for both the configurations with different thickness of the leaf springs. In the analysis of the simulations it turned out that the frequency difference between the metronomes influences the dynamics of the system significantly.

7.2 Recommendations

The experiments, performed with the setup, show that various synchronization regimes are possible. Although no efforts have been taken to exactly reproduce the findings of Huygens, regarding synchronization of pendulum clocks or the more recent work in Bennett et al. (2002) and Pantaleone (2002), the setup described in this report shows similar types of synchronization.

As the metronomes used in the experimental setup differ in both frequency and amplitude when oscillating uncoupled, the results are an example of synchronization between nonidentical systems. The observed effects of the differences between the metronomes are that no exact anti- or in-phase synchronization occurs, but with a small phase and amplitude difference. For approximate anti-phase synchronization this result can be understood physically in the following way. If the nonidentical metronomes would oscillate in exact anti-phase the resulting force from the metronomes on the platform is not zero, as it would be for two identical metronomes. As a result the platform is excited and will subsequently influence the metronomes as well. This drives the metronomes away from exact anti-phase synchronization.

It might be interesting to investigate experimentally and analytically how differences between the oscillators influence the synchronization that evolves, especially the phase and amplitude difference.

For further research and experiments with the setup, several recommendations can be given. First of all a better model of the metronomes, especially of the escapement, has to be considered. This might provide a better insight in the dynamics of the setup and the influence of the parameters can be understood better.

Regarding the chosen set of parameters of the setup, the value of the relative eigenfrequency of the platform needs to be evaluated. So far only experiments have been performed with either the relative eigenfrequency around the frequency of the metronomes or above it. No experiments have been run with an eigenfrequency significantly lower than the metronomes. This configuration

is used in Pantaleone (2002), where in-phase synchronization is prevalent over anti-phase synchronization. Possibly this type of synchronization can be found in the setup as well.

For the demonstration of synchronization the setup performs very well, however for analysis of the dynamics affecting synchronization, the setup is less well suited. The problem is located in the metronomes, whose dynamics is not understood completely, resulting in a model that does not match the measurements very well. A solution would be to design a new setup for which the following recommendations can be given. Although never a goal in this project, the possibility to actuate the pendulums and platform for control strategies is included in the ideas for a new setup.

- Replace the metronomes by pendula connected to an electrical motor. The energy input can then have an arbitrary form, which makes eg. any steady state amplitude of the oscillations possible.

- Design the pendula so that they have an equal eigenfrequency and can be adjusted in steps of $\pm 1‰$ of the relative frequency difference. The adjustment should be reproducible.

- Variation of the stiffness and damping of the platform should be made possible through the proposed actuation. Values of the relative eigenfrequency between at least 0.5 to 2 are advisable.

- The exact frequency of the pendula is not of interest, however it should be chosen so that appropriate relative eigenfrequencies of the platform are obtainable. For the current setup the frequency of the pendula should be increased a factor two to reach a relative eigenfrequency of the platform of 0.5.

- Replace the measurement of the translation of the platform by a different method than the LASER vibrometer. This should solve the problems of the relative measurement, ie. the zero position is unknown and drift occurs during long measurements.

- In the current setup the translation of the platform is limited to approximately 1-2 mm, which suffices for the performed experiments. As only for small oscillations the assumed linearity of the model is appropriate. However if larger oscillations are necessary, either the model for the platform should be adopted or the setup should be changed to take care or avoid nonlinear response of the platform.

- When designing the setup and cables, eg. power to the electromotors, have to run from the platform to the supporting frame, take into account that nonlinear damping can arise.

- Although the design of the leaf springs does show linear behavior, a proper constructive design is advisable. Points of attention are the restriction of the degrees of freedom, stiffness perpendicular to the direction of translation and linearity of the wanted stiffness and damping.

Bibliography

Appleton, E. (1922), 'The automatic synchronization of triode oscillators', *Proc. Cambridge Phil. Soc. (Math. and Phys. Sci.)* **21**, 231–248.

Applications of magnetic position sensors (2002), Technical report, Honeywell. http://www.magneticsensors.com, consulted: September 2004.

Bennett, M., Schatz, M., Rockwood, H. & Wiesenfeld, K. (2002), 'Huygens's clocks', *Proc. R. Soc. Lond. A* **458**(2019), 563–579.

Buck, J. (1988), 'Synchronous rhythmic flashing of fireflies. ii.', *Quaterly review of biology* **63**(3), 265–289.

De Kraker, B. & Van Campen, D. H. (2001), *Mechanical vibrations*, Shaker Publishings.

Fenner, R. T. (1989), *Mechanics of solids*, Blackwell Scientific.

Fröberg, C.-E. (1970), *Introduction to numerical analysis*, 2nd edn, Addison-Wesley, London.

Gelb, A., Kasper, J. F., Nash, R. A., Price, C. F. & Sutherland, A. A. (2001), *Aplied optimal estimation*, 16th edn, MIT Press.

Gray, C. M., König, P., Engel, A. K. & Singer, W. (1989), 'Oscillatory responses in cat visual cortex exhibit inter-columnar synchronization which reflects global stimulus properties', *Nature* **338**(6213), 334–337.

Huygens, C. (1893), *Oeuvres complétes de Christiaan Huygens*, Vol. 5, Martinus Nijhoff. Includes works from 1665.

Huygens, C. (1932), *Oeuvres complétes de Christiaan Huygens*, Vol. 17, Martinus Nijhoff. Includes works from 1651-1666.

Huygens, C. (1986), *Christiaan Huygens' the pendulum or geometrical demonstrations concerning the motion of pendula as applied to clocks (translated by R. Blackwell)*, Iowa State University Press, Ames, Iowa.

Kreyszig, E. (1993), *Advanced engineering mathematics*, 7th edn, John Wiley & Sons.

Linear/angular/rotary displacement sensors (2003), Technical report, Honeywell. http://www.magneticsensors.com, consulted: September 2004.

Nørgaard, M., Poulsen, N. K. & Ravn, O. (2000), 'New developments in state estimation for nonlinear systems', *Automatica* **36**(11), 1627–1638.

Pantaleone, J. (2002), 'Synchronization of metronomes', *American Journal of Physics* **70**(10), 992–1000.

Pikovsky, A., Rosenblum, M. & Kurths, J. (2001), *Synchronization*, Cambridge University Press.

Rosielle, P. & Reker, E. (2000), *Constructieprincipes 1*, Technische Universiteit Eindhoven. Lecture notes.

Von Der Malsburg, C. (1999), 'The what and why of binding: The modeler's perspective', *Neuron* **24**(1), 95–104.

Yoder, J. G. (1988), *Unrolling Time*, Cambridge University Press.

Ziemer, R. E. & Tranter, W. H. (2002), *Principles of Communications*, 5th edn, John Wiley & Sons.

Appendix A

Nonlinear state estimation

For the estimation of the parameters of the metronomes in section 4.2 and the coupling strength in section 4.3 a nonlinear filter has been used, proposed in Nørgaard et al. (2000). The structure of the estimator is discussed in this appendix.

Consider the following nonlinear discrete model which state is to be estimated

$$
\begin{align}
x_{k+1} &= f(x_k, u_k, v_k), & \text{(A.1)}\\
y_k &= g(x_k, w_k) & \text{(A.2)}
\end{align}
$$

with state x_k, input u_k, process noise v_k, output y_k and measurement noise w_k. The process and measurement noise are independent of each other, white and with normal probability distributions

$$
\begin{align}
v_k &\sim N(0, Q(k)) & \text{(A.3)}\\
w_k &\sim N(0, R(k)). & \text{(A.4)}
\end{align}
$$

The objective of the filter is to estimate the state of the system based on the model and past measurements. The *a priori* state $\bar{x}_k$ and error covariance $\bar{P}_k$ estimates are defined as

$$
\begin{align}
\bar{x}_k &= E[x_k|Y^{k-1}] & \text{(A.5)}\\
\bar{P}_k &= E[(x_k - \bar{x}_k)(x_k - \bar{x}_k)^\top|Y^{k-1}] & \text{(A.6)}
\end{align}
$$

where $Y^{k-1} = \begin{bmatrix} y_0 & y_1 & \dots & y_{k-1} \end{bmatrix}$ is a matrix containing the past measurements.

The *a posteriori* update of the state estimation $\hat{x}_k$ is performed in the Kalman filter so that the error covariance is minimized. This results in the Kalman gain K_k

$$
\begin{align}
K_k &= P_{xy}(k)P_y^{-1}(k) & \text{(A.7)}\\
\hat{x}_k &= \bar{x}_k + K_k[y_k - g(\bar{x}_k, w_k)] & \text{(A.8)}
\end{align}
$$

where

$$
\begin{align}
\bar{y}_k &= E[y_k|Y^{k-1}] & \text{(A.9)}\\
P_{xy}(k) &= E[(x_k - \bar{x}_k)(y_k - \bar{y}_k)^\top|Y^{k-1}] & \text{(A.10)}\\
P_y(k) &= E[(y_k - \bar{y}_k)(y_k - \bar{y}_k)^\top|Y^{k-1}]. & \text{(A.11)}
\end{align}
$$

The corresponding *a posteriori* update of the covariance matrix $\hat{P}_k$ is

$$\hat{P}_k = E[(x_k - \hat{x}_k)(x_k - \hat{x}_k)^\top | Y^k] = \bar{P}_k - K_k P_y(k) K_k^\top. \tag{A.12}$$

As for nonlinear systems calculation of the expectations is in most cases difficult, the state and output equations are approximated. The filter proposed in Nørgaard et al. (2000), which is utilized in this report, solves this problem by making use of polynomial approximations and statistically decoupling of the stochastic vectors. In particular, a multidimensional extension of Stirling's interpolation formula is used which is introduced in appendix B. Secondly a linear transformation is used which performs a stochastic decoupling. For eg. state x_k this is done by calculating a Cholesky factor of the covariance P_x

$$P_x = S_x S_x^\top \tag{A.13}$$

so that the following applies for the transformed stochastic vector $z = S_x^{-1} x$

$$E[(z - E[z])(z - E[z])^\top] = I, \tag{A.14}$$

where I is the unity matrix.

The following four square Cholesky factorizations are defined

$$\begin{aligned} Q = S_v S_v^\top, \quad & R = S_w S_w^\top \\ \bar{P} = \bar{S}_x \bar{S}_x^\top, \quad & \hat{P} = \hat{S}_x \hat{S}_x^\top \end{aligned} \tag{A.15}$$

of which S_v and S_w can be calculated in advance, the other two $\bar{S}_x$ and $\hat{S}_x$ are updated during application of the filter. Using the first order truncated, indicated by superscript (1), Stirling's polynomial approximation the following matrices can be defined

$$S_{x\hat{x}}^{(1)}(k) = \{ S_{x\hat{x}}^{(1)}(k)_{(i,j)} \} = \\ \{ (f_i(\hat{x}_k + h\hat{s}_{x,j}, u_k, \bar{v}_k) - f_i(\hat{x}_k - h\hat{s}_{x,j}, u_k, \bar{v}_k))/2h \} \tag{A.16}$$

$$S_{xv}^{(1)}(k) = \{ S_{xv}^{(1)}(k)_{(i,j)} \} = \\ \{ (f_i(\hat{x}_k, u_k, \bar{v}_k + h\hat{s}_{v,j}) - f_i(\hat{x}_k, u_k, \bar{v}_k - h\hat{s}_{v,j}))/2h \} \tag{A.17}$$

$$S_{y\bar{x}}^{(1)}(k) = \{ S_{y\bar{x}}^{(1)}(k)_{(i,j)} \} = \\ \{ (g_i(\bar{x}_k + h\bar{s}_{x,j}, \bar{w}_k) - g_i(\bar{x}_k - h\bar{s}_{x,j}, \bar{w}_k))/2h \} \tag{A.18}$$

$$S_{yw}^{(1)}(k) = \{ S_{yw}^{(1)}(k)_{(i,j)} \} = \\ \{ (g_i(\bar{x}_k, \bar{w}_k + hs_{w,j}) - g_i(\bar{x}_k, \bar{w}_k - hs_{w,j}))/2h \} \tag{A.19}$$

where $\bar{s}_{x,j}$ denotes the jth column of $\bar{S}_x$ and similarly for the other matrices.

The update of the *a priori* error covariance matrix can be written as

$$\bar{P}(k+1) = \bar{S}_x(\bar{S}_x)^\top = S_{x\bar{x}}^{(1)}(k)(S_{x\bar{x}}^{(1)})^\top + S_{xv}^{(1)}(k)(S_{xv}^{(1)})^\top \tag{A.20}$$

where the (rectangular and nontriangular) Cholesky factor can be found as

$$\bar{S}_x(k+1) = \begin{bmatrix} S_{x\bar{x}}^{(1)}(k) & S_{xv}^{(1)}(k) \end{bmatrix}. \tag{A.21}$$

This matrix must be converted to a square Cholesky factor for further use, for example by Householder triangularization.

A similar matrix exists for $P_y(k)$ where

$$S_y(k) = \begin{bmatrix} S_{y\bar{x}}^{(1)}(k) & S_{yw}^{(1)}(k) \end{bmatrix}, \tag{A.22}$$

which must also be converted to a square Cholesky factor.

Now the Kalman gain K_k can be calculated as

$$K_k = \bar{S}_x(k)(S_{y\bar{x}}(k))^\top (S_y(k)S_y(k)^\top)^{-1}. \tag{A.23}$$

Finally the *a posteriori* matrix $\hat{P}(k)$ can be updated by triangularization of the following matrix

$$\hat{S}_x(k) = \begin{bmatrix} \bar{S}_x(k) - K_k S_{y\bar{x}}^{(1)}(k) & K_k S_{yw}^{(1)}(k) \end{bmatrix}. \tag{A.24}$$

In the above description of the filter a first order truncated Stirling's polynomial approximation is given, whereas the filter used for the estimation of the parameters, uses a second order approximation. This does not change the structure of the filter, but does complexify the various equations. The detailed equations of this filter can be found in Nørgaard et al. (2000).

Finally it can be remarked that while the estimator introduced above, assumes discrete updates of the dynamical model, the model proposed in chapter 3 is a continuous time model. Using a fourth order Runge-Kutta method, Kreyszig (1993) the continuous model is discretized in the implementation of the filter.

Appendix B

Stirling's interpolation formula

The Stirling's interpolation formula is introduced in this appendix. First the one dimensional case is given and after that the multidimensional case. A more detailed description can be found in Fröberg (1970).

A one dimensional, analytic function $f(x)$ can be approximated around the point $\bar{x}$ with the Stirling's approximation formula by

$$
\begin{aligned}
f(x) = f(\bar{x} + ph) = f(\bar{x}) + p\mu\delta f(\bar{x}) + \frac{p^2}{2!}\delta^2 f(\bar{x}) + \begin{bmatrix} p+1 \\ 3 \end{bmatrix} \mu\delta^3 f(\bar{x}) \\
+ \frac{p^2(p^2-1)}{4!}\delta^4 f(\bar{x}) + \begin{bmatrix} p+2 \\ 5 \end{bmatrix} \mu\delta^5 f(\bar{x}) + \ldots
\end{aligned}
$$

(B.1)

where h is a selected interval length and the operations δ and μ are defined as

$$
\delta f(x) = f(x + h/2) - f(x - h/2) \tag{B.2}
$$

$$
\mu f(x) = \frac{1}{2}\big(f(x + h/2) + f(x - h/2)\big). \tag{B.3}
$$

For practical use only the first or second order polynomial approximations are used and (B.1) can be approximated by

$$
f(x) \approx f(\bar{x}) + f'_{DD}(\bar{x})(x - \bar{x}) + \frac{f''_{DD}(\bar{x})}{2!}(x - \bar{x})^2 \tag{B.4}
$$

where

$$
f'_{DD}(\bar{x}) = \frac{f(\bar{x} + h) - f(\bar{x} - h)}{2h} \tag{B.5}
$$

$$
f''_{DD}(\bar{x}) = \frac{f(\bar{x} + h) + f(\bar{x} - h) - 2f(\bar{x})}{h^2}. \tag{B.6}
$$

When restricted to second order polynomials, the interpolation formula can be written for the multidimensional case, where $x \in \mathbb{R}^n$ is a vector and $y = f(x)$ a

vector function, as

$$y \approx f(\bar{x}) + \tilde{D}_{\Delta x} f + \frac{1}{2!} \tilde{D}^2_{\Delta x} f \qquad (B.7)$$

where

$$\tilde{D}_{\Delta x} f \quad = \quad \frac{1}{h} \left(\sum_{p=1}^{n} \Delta x_p \mu_p \delta_p \right) f(\bar{x}) \qquad (B.8)$$

$$\tilde{D}^2_{\Delta x} f \quad = \quad \frac{1}{h^2} \left(\sum_{p=1}^{n} \Delta x_p^2 \delta_p^2 \sum_{p=1}^{n} \sum_{\substack{q=1 \\ q \neq p}}^{n} \Delta x_p \Delta x_q (\mu_p \delta_p)(\mu_q \delta_q) \right) f(\bar{x}) \quad (B.9)$$

and

$$\delta_p f(\bar{x}) = f(\bar{x} + \tfrac{1}{2} h e_p) - f(\bar{x} - \tfrac{1}{2} h e_p) \qquad (B.10)$$

and e_p is the pth unit vector. The average operator μ_p is extended in a similar way.

Appendix C

Complex demodulation

The characteristic features of oscillating signals are the amplitude and phase. Using the Hilbert transform it is possible to derive these signals from a response $y(t)$ in the time domain Ziemer & Tranter (2002). The Hilbert transform $\tilde{y}(t)$ can be considered as a filter that shifts the phase of all frequency components by $-\pi/2$ radians and is defined as

$$\mathbf{H}[y(t)] = \tilde{y}(t) = \frac{1}{\pi t} * y(t) = \frac{1}{\pi} \int_{-\infty}^{\infty} \frac{y(\tau)}{t - \tau} d\tau \qquad \text{(C.1)}$$

Using the Hilbert transform the signal can be written in its analytic signal form $Y(t)$

$$\begin{aligned} Y(t) &= y(t) + j\tilde{y}(t) = A(t)\exp(j\psi(t)) \\ \tilde{y}(t) &= \mathbf{H}[y(t)], \end{aligned} \qquad \text{(C.2)}$$

where $A(t)$ is the envelope signal (amplitude) and $\psi(t)$ is the instantaneous phase of the vibration. These two signals can easily be calculated from the analytic signal by

$$\begin{aligned} A(t) &= \sqrt{y^2(t) + \tilde{y}^2(t)} \\ \psi(t) &= \arctan(\tilde{y}(t)/y(t)) \end{aligned} \qquad \text{(C.3)}$$

Appendix D

Article Chaos'06

Article submitted to Chaos'06, the first IFAC Conference on Analysis and Control of Chaotic Systems, which will be held June 28-30 2006 in Reims, France

A study of Huijgens' synchronization. Experimental results

W.T. Oud[1], H. Nijmeijer[1], and A.Yu. Pogromsky[1]

Eindhoven University of Technology, Department of Mechanical Engineering, Eindhoven, The Netherlands

1 Introduction

One of the first scientifically documented observations of synchronization is by the Dutch scientist Christiaan Huygens. In the 17th century maritime navigation called for more accurate clocks in order to determine the longitude of a ship. Christiaan Huygens' solution for precise timekeeping was the invention of the pendulum clock [15] with cycloidal-shaped plates to confine the pendulum suspension. Those plates resulted in isochronous behavior of the pendulum independent of the amplitude and were genius invention of that time. During time Huygens was bound to his home due to illness he observed that two pendulum clocks attached to the same beam supported by chairs would swing in exact opposite direction after some time [8, 9, 10]. A drawing made by Christiaan Huygens is given in figure 1. Disturbances or different initial positions did not affect the synchronous motion which resulted after about half an hour. This effect which Huygens called *"sympathie des horloges"* is nowadays known as synchronization and is characterized by [12] as *"an adjustment of rhythms of oscillating objects due to their weak interaction"*. The oscillating objects in Huygens' case are two pendulum clocks and are weakly coupled through translation of the beam.
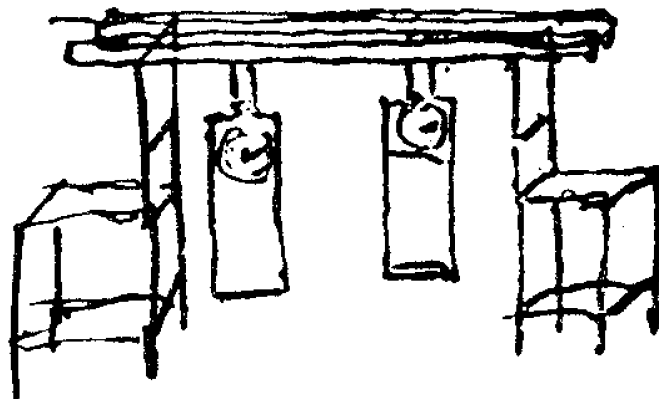

Fig. 1: Drawing by Christiaan Huygens of two pendulum clocks attached to a beam which is supported by chairs. Synchronization of the pendulums was observed by Huygens in this setup. From [9]

Many more cases of synchronization have been identified in nature and technology around us [14]. Two striking examples in biology are the synchronized flashing of fireflies [5] or synchronization of neurons in the brain when performing perceptual tasks. Synchronization is also found in technology, for example the frequency synchronization of triode generators. These generators were the basic

elements of early radio communication systems [3, 6]. Using synchronization it is possible to stabilize the frequency of a high power generators and there are more other applications we are unable to mention in this paper.

Three centuries later the phenomenon of synchronizing driven pendula is, to our best knowledge, repeated twice experimentally. In the first research by Bennett, Schatz, Rockwood and Wiesenfeld [4], one has tried to accurately reproduce the findings of Huygens in an experimental setup consisting of two pendulum clocks attached to a free moving cart. The results of this experiment confirm the documented observations of Christiaan Huygens. A rather simple but interesting experiment is described by Pantaleone [11], where the synchronization of two metronomes is discussed, which are coupled by a wooden board rolling on soda cans. The metronomes in this setup would synchronize most of the time with in phase oscillations.

The research presented in this paper is inspired by the observations of Christiaan Huygens, the work of Bennett et al. and Pantaleone. The main objective is to perform and analyze synchronization experiments with a setup consisting of driven pendula. Particular attention is paid to different syncronization regimes that can be observed in this situation : anti-phase, observed by Huygens, in-phase: observed by Blekhman and explained with the van der Pol equation for each pendulum and possible intermediate regimes.

The paper is organized as follows. First the design of the setup and the measurement methods are discussed and the mathematical model describing the setup is introduced. Then the synchronization experiments are discussed. Finally, conclusions are drawn and recommendations for further research are given.

2 Experimental setup

The experimental setup consists of two metronomes coupled by a platform which can translate horizontally. The metronomes are made by Wittner, type Maelzel (series 845). The platform is suspended by leaf springs, which allows a frictionless horizontal translation. A photograph of the experimental setup is given in figure 2.
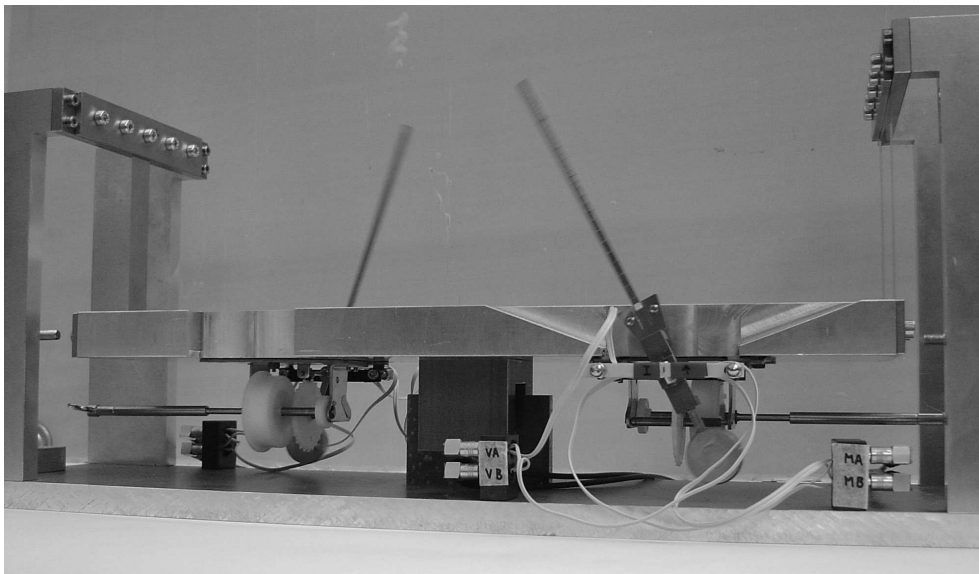

Fig. 2: Photograph of the setup.

2.1 Metronomes

The metronomes which are normally used for indicating a rhythm for musicians consist of a pendulum and a driving mechanism, called the escapement. The energy lost due to friction is compensated by this escapement. The escapement consists of a spring which loads on a toothed wheel. These teeth push alternately one of the two cams on the axis of the pendulum. Each time the teeth hit a cam a tick is produced, the typical sound of mechanical metronomes. The frequency of the metronomes can be adjusted with a contra weight attached to the upper part of the pendulum. Variation of the frequency between 2.4 rad/s and 10.8 rad/s is possible with the weight attached, without it the frequency of the metronomes increases to 12.3 rad/s. The amplitude of the metronome's oscillations cannot be influenced, however at increasing frequencies the amplitude decreases.

2.2 Platform

The platform does not only act as a support for the metronomes but because of its horizontal translation it couples the dynamics of both metronomes as well. In order to keep the equations of motion of the total system simple a suspension with linear stiffness and damping is desired. As long as the translation of the platform is not too large (mm range) the use of leaf springs makes a frictionless translation possible with linear stiffness and damping properties [13]. In order to calculate the necessary dimensions for leaf springs the following estimates have been used. The stiffness of a leaf spring can be estimated by assuming it behaves as two bars clamped at one side. For small deflections the stiffness of bar clamped at one side is given by [7]

$$k = \frac{Ehb^3}{4L^3},\tag{1}$$

where E is the elastic modulus, h the width, b the thickness and L the length of the bar. The leaf spring has a stiffness equal to (1) since both halves of the leaf spring take half the deflection and half the force, thus equal to the stiffness of a single sided clamped beam. The eigenfrequency of the platform in rad/s is estimated by

$$\Omega = \sqrt{\frac{Ehb^3}{4(l/2)^3 M} + \frac{g}{l}}\tag{2}$$

where l is the length of the leaf spring, M the mass of the platform and g the constant of gravity. For the setup the following dimensions for the leaf springs are chosen: l=80 mm, b=0.4 mm and h=15+15+10 mm (three leaf springs). The constants are $E = 200 \cdot 10^9$ kg/m/s^2 and g=9.81 m/s^2. The platform has a mass of 2.35 kg which results in an eigenfrequency of 31.2 rad/s.

2.3 Measurements

In the setup the angle of the metronomes and the translation of the platform are of interest. Since alteration of the dynamics of both the metronomes and the platform should be avoided, contactless measurement methods have been chosen. All signals are recorded using a Siglab data acquisition system, model 20-42. First the measurement of the metronomes is discussed, secondly that of the translation of the platform.

The angle of the metronomes is measured using a sensor based on the anisotropic magnetoresistance (AMR) principle [1], [2]. The resistance of AMR materials changes when a magnetic field is applied. Above a minimal field strength the magnetization of the material aligns with the external field and the following relation holds for the resistance R

$$R \sim \cos^2 \theta\tag{3}$$

where θ is the angle between the magnetic field and the current through the resistor. By combining four AMR resistors in a bridge of Wheatstone a change in resistance is converted to a voltage

difference. Two of these bridges of Wheatstone are located in the sensor, but are rotated 45° degrees with respect to each other. As a result the voltage difference of bridges A and B can be written as

$$\Delta V_A = V_s S \sin 2\theta \, , \; \Delta V_B = V_s S \cos 2\theta \tag{4}$$

where V_s is the voltage supplied to the bridges and S is the AMR material constant. The angle θ can be calculated from these signals by

$$\theta = \tfrac{1}{2} \arctan(\Delta V_A / \Delta V_B) \tag{5}$$

regardless of the value of voltage V_s and constant S. Due to manufacturing tolerances the bridges will show an offset when no magnetic field is applied. This offset can be corrected in software when both signals are recorded.

The velocity of the platform is measured using a Polytec Vibrometer, type OFV 3000 with a OFV 302 sensorhead. The measurement is based on the Doppler shift of a laser beam reflected on the platform.

3 Mathematical model of the setup

Assuming the setup consists of rigid bodies the equations of motion can be derived using Lagrangian mechanics. The generalized coordinates are chosen as

$$\underline{q}^T = [\theta_1, \theta_2, x] \tag{6}$$

which are the angles of the pendulums from the vertical and the translation of the platform. The kinetic energy $T(\underline{q}, \underline{\dot{q}})$ of the system can be expressed as

$$T(\underline{q}, \underline{\dot{q}}) = \tfrac{1}{2} m_1 \dot{\mathbf{r}}_1 \cdot \dot{\mathbf{r}}_1 + \tfrac{1}{2} m_2 \dot{\mathbf{r}}_2 \cdot \dot{\mathbf{r}}_2 + \frac{1}{2} M \dot{\mathbf{r}}_3 \cdot \dot{\mathbf{r}}_3 \tag{7}$$

where r_1, r_2 and r_3 are respectively the translation of the center of mass of pendulum 1, 2 and the platform, m_1 and m_2 are the mass of pendulum 1 and 2, l_1 and l_2 the lengths of the center of mass to the pivot point of pendulum 1 and 2, M is the mass of the platform and

$$\mathbf{r}_1 = (x + l_1 \sin \theta_1) \cdot \mathbf{e}_1 - l_1 \cos \theta_1 \cdot \mathbf{e}_2 \tag{8a}$$
$$\mathbf{r}_2 = (x + l_2 \sin \theta_2) \cdot \mathbf{e}_1 - l_2 \cos \theta_2 \cdot \mathbf{e}_2 \tag{8b}$$
$$\mathbf{r}_3 = x \cdot \mathbf{e}_1 \tag{8c}$$

The potential energy $V(\underline{q})$ of the system is given by

$$V(\underline{q}) = m_1 g l_1 (1 - \cos \theta_1) + m_2 g l_2 (1 - \cos \theta_2) + \tfrac{1}{2} k x \tag{9}$$

where g is the constant of gravity and k is the spring stiffness of the platform. The generalized forces $\underline{Q}^{nc}$ include viscous damping in the hinges of the pendulums and the platform and the torque $f_i(\theta_i, \dot{\theta}_i)$ exerted by the escapement mechanism on the pendulums and can be written as

$$\underline{Q}^{nc} = \begin{bmatrix} f_1(\theta_1, \dot{\theta}_1) - d_1 \dot{\theta}_1 \\ f_2(\theta_1, \dot{\theta}_1) - d_2 \dot{\theta}_2 \\ -d_3 \dot{x} \end{bmatrix} \tag{10}$$

where d_i are the viscous damping constants of respectively the two pendulums and the platform. With Lagrange's equations of motions

$$\frac{d}{dt} \left(T_{,\underline{\dot{q}}} \right) - T_{,\underline{q}} + V_{,\underline{q}} = \left(\underline{Q}^{nc} \right)^T \tag{11}$$

the equations of motion for the system become

$$m_1 l_1{}^2 \ddot{\theta}_1 + m_1 l_1 g \sin\theta_1 + m_1 l_1 \cos(\theta_1)\ddot{x} + d_1 \dot{\theta}_1 = \mathrm{f}_1(\theta_1, \dot{\theta}_1)$$
$$m_2 l_2{}^2 \ddot{\theta}_2 + m_2 l_2 g \sin\theta_2 + m_2 l_2 \cos(\theta_2)\ddot{x} + d_2 \dot{\theta}_2 = \mathrm{f}_2(\theta_2, \dot{\theta}_2) \tag{12}$$
$$M\ddot{x} + d_3 \dot{x} + kx + \sum_{i=1}^{n} m_i l_i \left(\ddot{\theta}_i \cos\theta_i - \dot{\theta}_i^2 \sin\theta_i \right) = 0.$$

These equations for the metronomes can be simplified by dividing all terms by $m_i l_i{}^2$, which give for $i = 1, 2$

$$\ddot{\theta}_i + \omega_i{}^2 \sin\theta_i + \frac{1}{l_i} \cos(\theta_i)\ddot{x} + \frac{d_i}{m_i l_i{}^2}\dot{\theta}_i = \frac{1}{m_i l_i{}^2}\mathrm{f}_i(\theta_i, \dot{\theta}_i) \tag{13}$$

where $\omega_i = \sqrt{g/l_i}$.

The equations of motion can be written in dimensionless form using the following transformations. The dimensionless time is defined as $\tau = \omega t$ and the position of the platform as $y = x/l = x\omega^2/g$, where ω is the mean angular frequency of both pendulums. The derivatives of the angles with respect to the dimensionless time are written as

$$\frac{d\theta}{dt} = \frac{d\theta}{d\tau}\frac{d\tau}{dt} = \omega\theta', \quad \frac{d^2\theta}{dt^2} = \omega^2\theta''.$$

The equations of motion now become

$$\theta_i'' + \gamma_i^2 \cos\theta_i y'' + \gamma_i^2 \sin\theta_i + \delta_i\theta_i' = \epsilon_i\,\mathrm{f}(\theta_i, \theta_i'), \tag{14}$$
$$y'' + 2\Omega\xi y' + \Omega^2 y + \sum_{i=1}^{2} \beta_i\gamma_i^{-2}\left(\cos\theta_i\theta_i'' - \sin\theta_i\theta_i'^2 \right) = 0,$$

with coupling parameter $\beta_i = \frac{m_i}{M}$, scaled eigenfrequency of the metronomes $\gamma_i = \omega_i/\omega$, damping factor $\delta_i = \frac{d\omega_i{}^2}{m_i g}$, eigenfrequency of the platform $\Omega^2 = \frac{k}{M\omega^2}$ and damping ratio of the platform $\xi = \frac{d_3}{2\sqrt{kM}}$. The factor $\epsilon_i = \frac{\omega_i{}^4}{m_i g^2}$ will be set to 1 in further equations, since this factor can be taken into account in the model of the escapement.

3.1 Escapement

So far the escapement has been indicated by the function $\mathrm{f}(\theta, \theta')$. A close inspection of the metronomes shows that the escapement gives the pendulum a push when going upward. Without deriving an accurate mechanical model of the escapement mechanism this torque is approximated by the following normalized expression:

$$\mathrm{f}(\theta, \theta') = 0, \quad \text{if} \ \ \theta < \phi \lor \theta > \phi + \Delta\phi \tag{15}$$
$$\mathrm{f}(\theta, \theta') = \frac{1 - \cos(2\pi\frac{\theta-\phi}{\Delta\phi})}{2\Delta\phi},$$
$$\text{if} \ \ \phi \le \theta \le \phi + \Delta\phi \land \theta' > 0$$

where θ_1 and θ_2 are angles between which the mechanism works. In figure 3 the torque of the escapement is plotted versus time when the pendulum would follow a periodic trajectory.
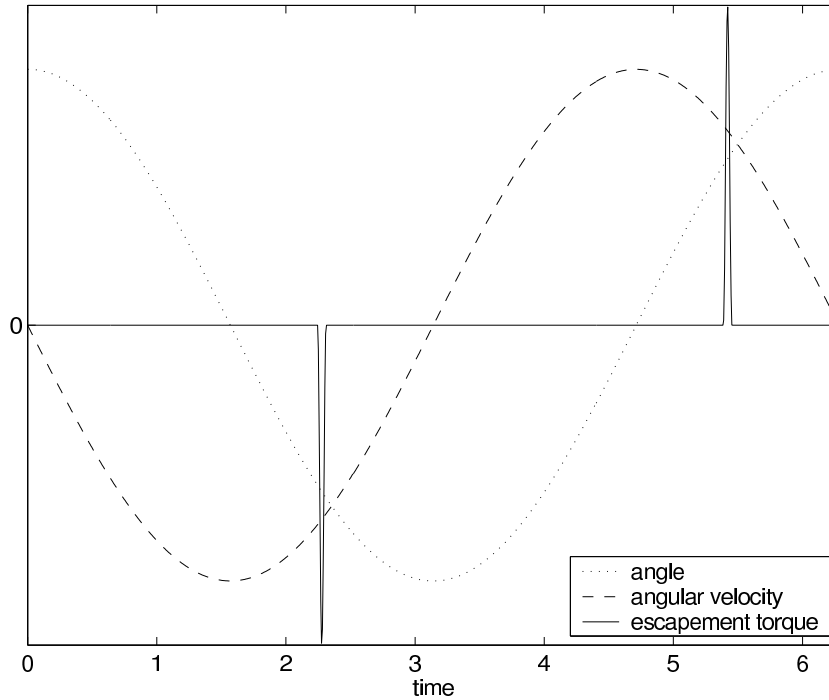
Fig. 3: The torque exerted by the escapement on the pendulum is plotted versus time together with the angle and velocity of the pendulum. The vertical axis is scaled in order to illustrate the torque more clearly.

4 Experimental results

Several experiments are performed in order to gain experience with the dynamics of the system. Parameters which can be varied in the experiment are the mass of the platform, the mass and frequency of the metronomes and the amount of damping in the system. Converted to the dimensionless parameters the influence of the physical parameters is:

$$\Delta = (\omega_1 - \omega_2)/\omega, \quad \omega = (\omega_1 + \omega_2)/2$$
$$\beta = m/M$$
$$\Omega = \sqrt{k/M}/\omega$$
$$\xi = d/2/\sqrt{kM}$$

The experiments show different phenomena, first of all when the damping of the platform is too small (< 2.0 kg/s) the pendulums hit the frame. These experiments are discarded since we want to avoid collisions in the experiments. Apparently, without enough damping the platform and consequently the metronomes are excited too much. For larger damping synchronization with different phase differences is observed. Three different types of responses can be identified, anti phase synchronization, intermediate (neither anti nor in) regime with a large amplitude difference of the angles of the metronomes and finally in phase synchronization.

4.1 Anti-phase synchronization

Experiments have been performed with the setup to show synchronization of the metronomes. The parameters that can be varied in the experimental setup are the frequency of the metronomes and the mass of the platform. The frequency of the metronomes is chosen as high as possible in order to reduce the time experiments will take. By adjusting the counterweights the frequency difference between

both metronomes is minimized, since too large a frequency difference will make synchronization impossible [4]. The second parameter that can be changed is the mass of the platform. Changing this influences the dynamics of the system in three ways. First, the coupling between the metronomes changes since the coupling parameter β is the ratio between the mass of the metronome's pendulum and the total mass of the platform. Secondly the relative eigenfrequency of the platform changes, increasing the mass of the platform lowers the eigenfrequency. Finally the relative damping factor of the platform depends on the mass.

In the experiments the frequency of metronome I is set to 10.565 rad/s and that of metronome II to 10.553 rad/s, which results in a mean frequency of $\omega = 10.559$ rad/s and a relative frequency difference of $\Delta = 1.1 \cdot 10^{-3}$. The mass of the platform is varied between 2.35 kg and 8.18 kg in five steps, resulting in a coupling parameter β varying between $19.5 \cdot 10^{-3}$ and $5.60 \cdot 10^{-3}$. For each choice of mass the experiments are started with several initial conditions. Since the metronomes need to be started by hand, reproducing the initial conditions exactly between experiments is impossible.

When the mass of the platform is varied, the following observations can be made from the experiments. For small mass the setup synchronizes to approximately constant phase for all initial conditions. When the mass of the platform increases the metronomes do not always synchronize anymore. When they do the phase difference is comparable to that in experiments with small mass of the platform.

A typical example of the experiments, in which synchronization for all initial conditions is observed, is depicted in figure 4, where the difference in phase of the metronomes, their amplitudes and the dimensionless velocity of the platform are plotted. The mass of the platform in this experiment is 2.35 kg, resulting in a coupling factor $\beta = 19.6 \cdot 10^{-3}$, dimensionless eigenfrequency $\Omega = 2.1$ and dimensionless damping factor $\xi = 7.9 \cdot 10^{-4}$. The resulting difference in phase between the metronomes, when they are synchronized, is approximately 0.8π with a variation of 0.1π. The amplitude of the oscillations of metronome II is larger than that of metronome I, which is also the case, and with comparable magnitude, when the metronomes run uncoupled. The difference is approximately 0.05 rad and the amplitude of metronome I and II is respectively about 0.80 and 0.85 rad. As the metronomes do not synchronize in exact anti-phase, the platform keeps oscillating. The amplitude of the dimensionless velocity of the platform is approximately 0.01.
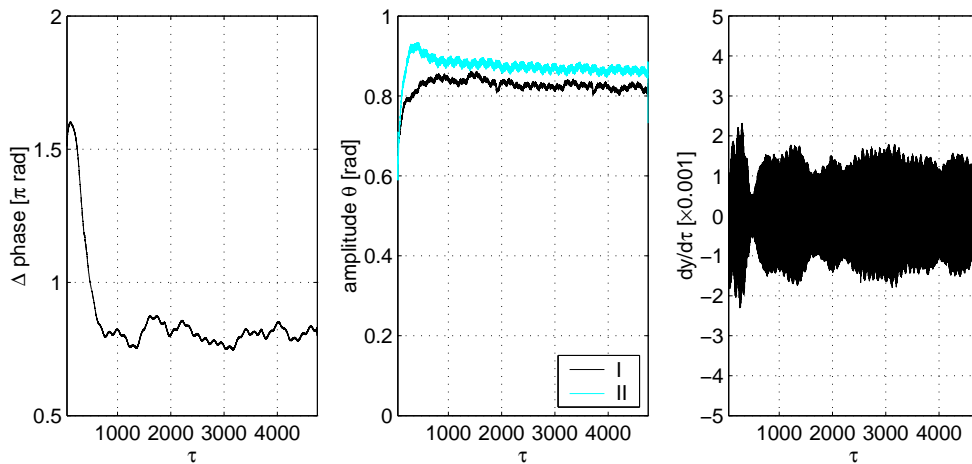

Fig. 4: A synchronization experiment in which phase synchronization can be observed. The dimensionless parameters are as follows in the experiment, $\Delta = 7.9 \cdot 10^{-4}$, $\beta = 0.020$, $\Omega = 2.1$ and $\xi = 7.8 \cdot 10^{-4}$. The mean phase difference between both metronomes is 0.80π after $\tau = 2000$, but a variation of about 10% can be seen around this value.

When the mass of the platform increases, the system does not always synchronizes to a constant phase. An example of such experiment is plotted in figure 5, where $M = 5.17$ kg and accordingly

$\beta = 8.9 \cdot 10^{-3}$, $\Omega = 1.6$ and $\xi = 6.8 \cdot 10^{-4}$. After approximately $\tau = 2000$ the system looses synchrony and the amplitude of the metronomes start oscillating. A similar phenomenon occurs in the experiment plotted in 6 with the same parameters but different initial conditions. In this experiment the metronomes seem to synchronize around $\tau = 1000$, then diverge, but synchronize again after $\tau = 2600$. However the length of the experiment is too short to be sure whether the metronomes will not desynchronize again.
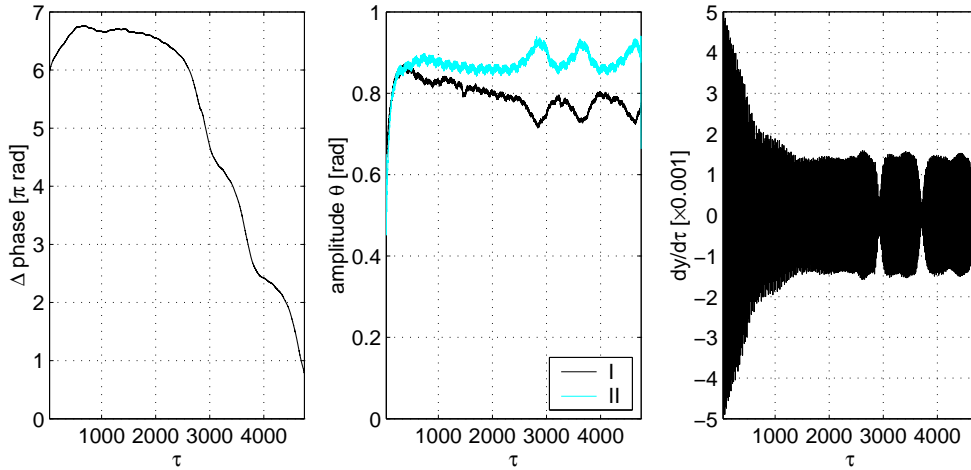

Fig. 5: Experiment with $\beta = 8.9 \cdot 10^{-3}$ in which synchronization is lost. When this happens the amplitudes of the metronomes diverge and start oscillating.
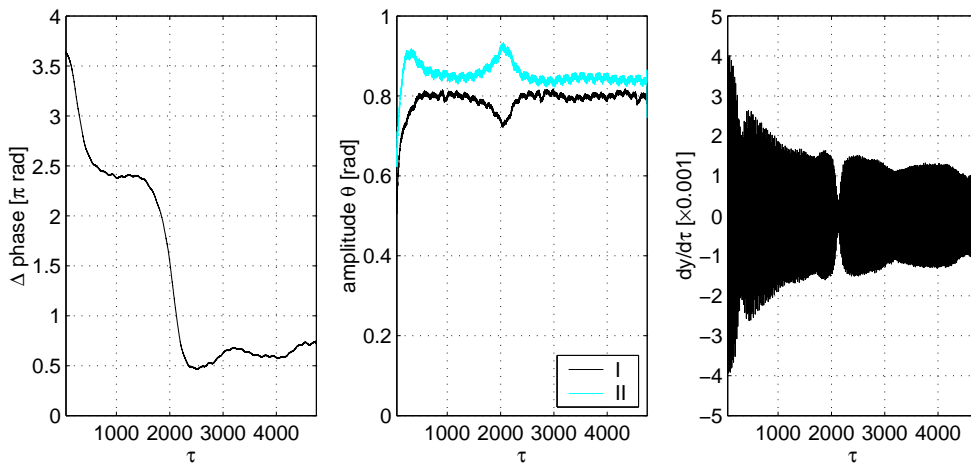

Fig. 6: After losing synchronization around $\tau = 2000$ the system synchronizes with a phase difference of 0.8π. The coupling factor in this experiment is $\beta = 8.9 \cdot 10^{-3}$.

In the performed experiments phase synchronization of two metronomes is visible, however the influence of disturbances in the system are clearly visible in the difference in phase of the metronomes. One of the disturbances acting on the system is the irregular operation of the escapement. Due to this the amplitude of the uncoupled metronomes also show a variation of about 10% when oscillating.

4.2 In- and anti-phase synchronization

In a slightly changed experimental setup more types of synchronization can be observed. Instead of leaf springs of 0.4 mm thickness, more flexible leaf springs with 0.1 mm thickness are used. With this change in the experimental setup the value of Ω is approximately 1. A major drawback of this value is that resonance of the platform is possible since the frequency of the platform matches that of the metronomes. When oscillations of the platform become too large, the metronomes will hit the frame. To prevent this, damping of the platform is increased using magnetic damping. The counterweights of the metronomes are removed in these experiments, as a result the frequency of the metronomes is increased, as well as the relative frequency difference compared to the previous experiments.

For a small coupling parameter the system synchronizes with approximate anti-phase, as can be seen in figure 7. The mass of the platform is 2.35 kg in this experiment, resulting in the following dimensionless parameters, $\beta = 16.6 \cdot 10^{-3}$, $\Omega = 0.96$ and $\xi = 7.8\%$. When the mass of the platform increases anti-phase synchronization does no longer occur, instead the metronomes synchronize in two different ways depending on the initial conditions. In figure 8 in-phase synchronization is obtained after starting the metronomes with approximate equal angles and in-phase. If the metronomes are started with anti-phase, the system synchronizes to a constant phase difference of about 0.65 and a large difference in amplitude between metronom I and II, this is shown in figure 9. In both figures the parameters of the system are $\beta = 8.56 \cdot 10^{-3}$, $\Omega = 0.94$ and $\xi = 4.2\%$.
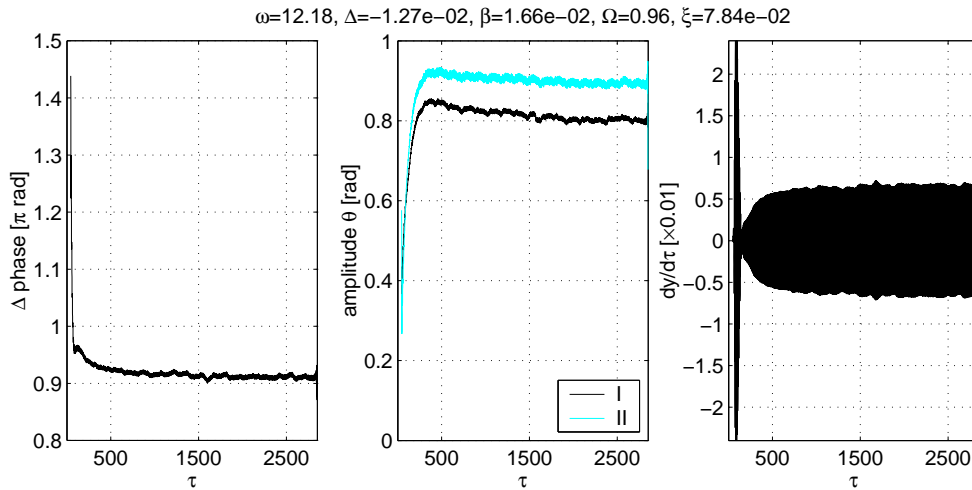

Fig. 7: Experiment in which the metronomes synchronize with approximate anti-phase.

5 Conclusions

This paper presents some experimental results on synchronization of two metronomes attached to a common beam that can move in horizontal direction. From those experiments it becomes evident that different synchronization regimes can (co-)exist depending on the system parameters. It is worth mentioning that we have observed from those experiments some intermediate seemingly chaotic regimes of oscillations. Further research will be devoted towards theoretical studies of those oscillations.
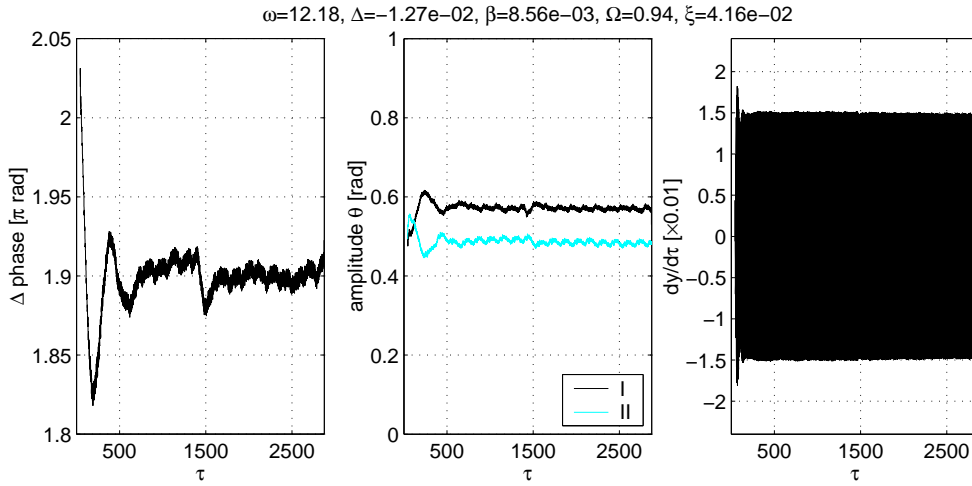
Fig. 8: For large enough mass of the platform and with the initial conditions close to in-phase synchronization, the metronomes synchronize in-phase.
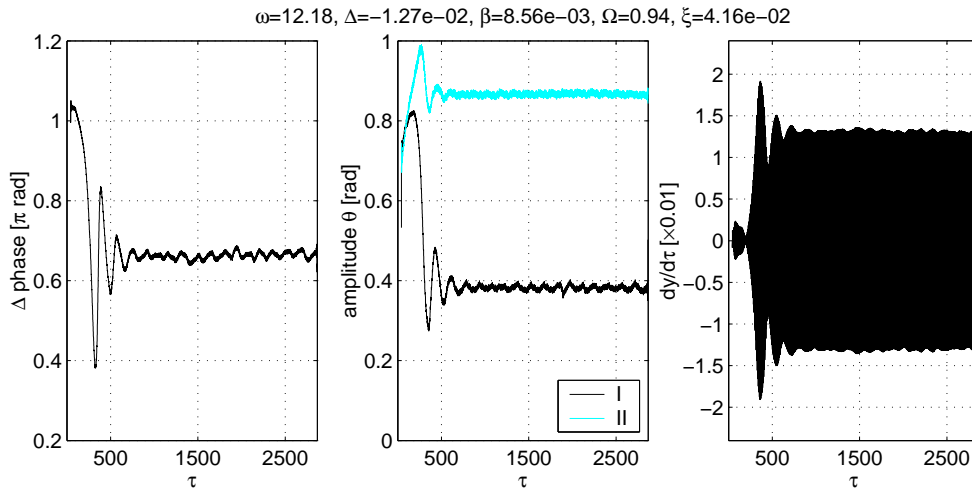

Fig. 9: The metronomes synchronize with a constant phase but a large difference in amplitude for equal parameters of the system as when in-phase synchronization is observed, the initial conditions differ however.

Acknowledgement

6 References

1. Applications of magnetic position sensors. Technical report, Honeywell, 2002.
2. Linear / angular / rotary displacement sensors. Technical report, Honeywell, 2003.
3. E.V. Appleton. The automatic synchronization of triode oscillators. *Proc. Cambridge Phil. Soc. (Math. and Phys. Sci.)*, 21:231–248, 1922.

4. Matthew Bennett, Michael Schatz, Heidi Rockwood, and Kurt Wiesenfeld. Huygens's clocks. *Proc. R. Soc. Lond. A*, 458(2019):563–579, jan 2002.
5. J. Buck. Synchronous rhythmic flashing of fireflies. ii. *Quaterly review of biology*, 63(3):265–289, 1988.
6. B. Van der Pol. Theory of the amplitude of free and forced triod vibration. *Radio Rev.*, 1:701–710, 1922.
7. Roger T. Fenner. *Mechanics of solids.* Blackwell Scientific, 1989.
8. Christiaan Huygens. *Oeuvres complétes de Christiaan Huygens*, volume 5. Martinus Nijhoff, 1893. Includes works from 1665.
9. Christiaan Huygens. *Oeuvres complétes de Christiaan Huygens*, volume 17. Martinus Nijhoff, 1932. Includes works from 1651-1666.
10. Christiaan Huygens. *Christiaan Huygens' the pendulum or geometrical demonstrations concerning the motion of pendula as applied to clocks (translated by R. Blackwell).* Iowa State University Press, Ames, Iowa, 1986.
11. James Pantaleone. Synchronization of metronomes. *American Journal of Physics*, 70(10):992–1000, oct 2002.
12. Arkady Pikosvky, Michael Rosenblum, and Jürgen Kurths. *Synchronization.* Cambridge University Press, 2001.
13. P.C.J.N Rosielle and E.A.G. Reker. Constructieprincipes 1. Technical report, Technische Universiteit Eindhoven, 2000.
14. Steven Strogatz. *Sync.* Hyperion, New York, 2003.
15. Joella G. Yoder. *Unrolling Time.* Cambridge University Press, 1988.

Samenvatting

Geïnspireerd door de observatie van synchronisatie van twee slingeruurwerken door Christiaan Huygens, is een vergelijkbare opstelling ontworpen en geanalyseerd in dit verslag. In plaats van pendulum klokken zijn metronomen gebruikt als oscillatoren in de opstelling. De koppeling tussen de metronomen is aangebracht door horizontale beweging van het platform waarop de metronomen bevestigd zijn.

Na beschrijving van het ontwerp van de opstelling en de gebruikte meetmethoden, is model geponeerd, waarmee het systeem is geanalyseerd. Dit model bestaat uit twee aangedreven slingers, bevestigd aan een massa, welke is verbonden met de vaste wereld met een lineaire veer en demper. Het echappement, wat voor energietoevoer in de metronomen zorgt, is gemodelleerd als een sinusvormige moment tussen twee vastgelegde hoeken. Alle parameters in het model zijn geïdentificeerd met een niet-lineair Kalman filter en de resultaten van de identificatie zijn gevalideerd.

Synchronisatie experimenten zijn uitgevoerd voor twee verschillende configuraties van het systeem. Ten eerste is synchronisatie van de metronomen bekeken, wanneer de relatieve eigenfrequentie van het platform ongeveer twee keer zo groot is als de natuurlijke frequentie van de metronomen. In deze situatie is alleen anti-fase synchronisatie waargenomen. Als de eigenfrequentie van het platform echter rond de frequentie van de metronomen ligt, is zowel anti- als in-fase synchronisatie mogelijk, afhankelijk van de parameters van het systeem. Tot slot zijn de bevindingen van de experimenten kwalitatief bevestigd in simulaties met het model.